







Relay interlayer synchronisation: invariance and stability conditions

Sarbendu Rakshit¹ , Fatemeh Parastesh² ,
Sayantan Nag Chowdhury¹ , Sajad Jafari² ,
Jürgen Kurths^{3,4,5}  and Dibakar Ghosh^{1,*} 

¹ Physics and Applied Mathematics Unit, Indian Statistical Institute, 203 B. T. Road, Kolkata 700108, India

² Department of Biomedical Engineering, Amirkabir University of Technology, 424 Hafez Avenue, Tehran 15875-4413, Iran

³ Potsdam Institute for Climate Impact Research, Telegraphenberg A 31, Potsdam, 14473, Germany

⁴ Department of Physics, Humboldt University Berlin, Berlin, 12489, Germany

⁵ Lobachevsky University of Nizhny Novgorod, Inst. of Inform. Technol., Nizhnij Novgorod 603950, Russia

E-mail: dibakar@isical.ac.in

Received 31 March 2020, revised 18 November 2021

Accepted for publication 22 November 2021

Published 14 December 2021



CrossMark

Abstract

In this paper, the existence (invariance) and stability (locally and globally) of relay interlayer synchronisation (RIS) are investigated in a chain of multiplex networks. The local dynamics of the nodes in the symmetric positions layers on both sides of the non-identical middlemost layer(s) are identical. The local and global stability conditions for this synchronisation state are analytically derived based on the master stability function approach and by constructing a suitable Lyapunov function, respectively. We propose an appropriate demultiplexing process for the existence of the RIS state. Then the variational equation transverse to the RIS manifold for demultiplexed networks is derived. In numerical simulations, the impact of interlayer and intralayer coupling strengths, variations of the system parameter in the relay layers and demultiplexing on the emergence of RIS in triplex and pentaplex networks are explored. Interestingly, in this multiplex network, enhancement of RIS is observed when a type of impurity via parameter mismatch in the local dynamics of the nodes is introduced in the middlemost layer. A common time-lag with small amplitude shift between the symmetric positions and central layers plays an important role for the enhancing of relay interlayer synchrony. This analysis improves our

*Author to whom any correspondence should be addressed.

Recommended by Mrs Natasha Leeper.

understanding of synchronisation states in multiplex networks with nonidentical layers.

Keywords: multiplex network, interlayer synchronisation, asymptotic stability, global stability analysis

Mathematics Subject Classification numbers: 34D06, 34C15, 35B40, 93D20, 93D05, 34D23.

(Some figures may appear in colour only in the online journal)

Contents

1. Introduction	682
2. Mathematical preliminaries	684
3. Mathematical model	685
4. Analytical results	687
4.1. Invariance of interlayer synchronisation	687
4.2. Stability of relay interlayer synchronisation state	688
4.3. Demultiplexing effect	693
5. Numerical illustrations for three-layer (i.e., $L = 1$) multiplex networks	695
5.1. Lorenz system	696
5.1.1. Relay interlayer synchronisation	696
5.1.2. Demultiplexing effect	701
5.2. Rössler system	703
6. Numerical results for five-layer (i.e., $L = 2$) multiplex network	705
6.1. Relay interlayer synchronisation	706
6.2. Demultiplexing effect	709
7. Conclusion and future perspectives	711
Acknowledgments	712
Appendix A. The proofs	713
A.1. Proof of lemma 1	713
A.2. Proof of lemma 3	713
A.3. Proof of lemma 4	714
A.4. Proof of lemma 14	714
A.5. Proof of theorem 15	715
References	716

1. Introduction

The study of complex networks is one of the focus of many scientists in various fields like mathematics, physics, biology, and engineering [1]. A complex network is often referred to as a set of large numbers of nodes interacting via links [2]. Real-world networks are developed from multiple types of connections [3]. A large class of engineering and natural systems, ranging from transportation networks to neuronal networks, are best represented by multilayer network architectures, namely a network composed of two or more different layers where the interaction between the nodes in a layer may differ from the other layers. In recent years,

researchers have paid much attention to multilayer networks to take advantage of considering diverse interactions in real networks [4]. A multiplex network is a special type of multilayer network in which each layer is composed of same number of nodes and each node of a layer is connected to its counterpart node in the adjacent layers through the interlayer links [3].

Most of the networks are supported by some internal dynamical processes. The study of the combined effect of the network structure and the dynamical property has great importance in several disciplines [5, 6]. The influence of network architecture and isolate node dynamics lead to the discovery of various interesting emergent phenomena in dynamical networks [7, 8]. Different collective behaviors are emerged in complex networks and synchronisation is one of the most important ones [9–11]. It is an emerging phenomenon in interacting dynamical systems, associated with many natural events [12, 13]. There are extensive numerical and analytical studies concerning synchronisation in different applications including biology, neuroscience, engineering, and economics [14–16].

Various types of synchronisation behaviors have been observed in multiplex networks such as cluster synchronisation [17], antiphase synchronisation [18], explosive synchronisation [19], chimera states [20–22], intralayer synchronisation [23], interlayer synchronisation [24], and relay interlayer synchronisation (RIS) [25]. Recently, analytical conditions for synchronisation of a multiplex network with time-varying intralayer connections has been studied [26, 27]. The occurrence of solitary states has been also analyzed [28] in multiplex structure with negative and positive interactions, where one or some of the units of the network oscillate differently from the other synchronised units. There were few studies [23, 29–33] done on synchronisation in heterogeneous coupled oscillator which is ubiquitous in nature. Plotnikov *et al* [32] observed enhancing synchronisation by enlarging the heterogeneity in a network of FitzHugh–Nagumo neurons. Gambuzza *et al* [23] considered a multiplex network composed of a layer of disconnected oscillators and a layer of connected oscillators which had a mismatch in their frequencies.

Recently, an idea has been proposed in reference [34] for multiplex adaptive networks to produce and stabilise several phase cluster states. It has been shown that symmetric multiplexing can induce several stable partial synchronisation patterns in circumstances where these states are neither stable nor even exist in a mono-layer network. The control technique of chimera states has been investigated for a multiplex network consisting of FitzHugh–Nagumo neurons by exploiting the multiplex structure [35]. In a multilayer network consisting of electronic Colpitts oscillators, the cluster synchronisation states are experimentally investigated by varying the interaction strength [36]. The emergence and stability of the cluster synchronisation state are investigated in multilayer network [37], and experimentally validate the result in electronic oscillators. Group consensus problem has been considered in multilayer network architecture [38], where the symmetries of the multilayer network determine the pattern of such dynamics. Here, the stability of group consensus was determined by decomposing the dynamics of the network into parallel and orthogonal components along the consensus manifold.

Initially, the interlayer synchronisation was studied in a multiplex network with two identical layers and the necessary conditions for the existence and stability of such state are analytically derived [24]. Later, Leyva *et al* [39] investigated the analytical approximate solution for interlayer synchronisation in two-layer multiplex networks with different intralayer structural connectivities. However, in most of the studies on synchronisation in multiplex networks, only two interacting layers were considered, and the study by considering more than two layers is in its infancy. Moreover, the effect of a non-identical layer on the interlayer synchronisation state in a multiplex network remains unclear still now.

Relay synchronisation in a network is an important feature which allows distant coordination between two indirectly connected oscillators [40]. Enhancing relay synchrony was

previously studied in a chain of mutually coupled oscillators using dynamic relaying [40]. Latterly, a mechanism to accomplish stable remote synchronisation state has been derived in a network of heterogeneous Kuramoto oscillators [41]. This phenomenon was numerically reported in multiplex network [42], where interlayer synchronisation occurs between distant layers mediated by a relay layer, and experimentally validated the numerical findings by means of a three-layer multiplex electronic circuits. Recently, this phenomenon is termed as RIS [25] for a three-layer network of interacting FitzHugh–Nagumo oscillators and the robustness of relay synchronisation of chimera state is also studied. The effect of connectivity in the remote and relay layers on the relay synchronisation in triplex neuronal networks is also discussed. Later, relay synchronisation of chimeras in triplex network is observed between the outer layers and time-delay in the interlayer coupling functions controls the chimera patterns [43]. Here the local dynamics of the nodes in each layers are identical and the effect of topology in the relay layer on the chimera relay synchronisation state is discussed. Rybalova *et al* [44] explored the relay synchronisation of chimera and solitary states in triplex network where the spatiotemporal dynamics of the relay layer is completely different from the outer layers. They also discussed the role of relay layer structure on the complete and relay synchronisation in heterogeneous triplex network of chaotic maps. Relay synchronisation of chimera states is also observed in triplex network of discrete maps where the transition from phase to amplitude chimera states observed [45]. Recently, Rakshit *et al* [46] explored the existence and stability conditions for interlayer synchronisation manifold for two-layer stochastic multiplex hypernetwork where the intralayer and interlayer connections are vary with respect to time. They also proved that intralayer synchronisation is not possible due to stochastic interlayer connections and the obtained existence and stability conditions are valid for any rewiring probabilities. In spite of these studies, we have observed that the invariance and stability properties of the RIS state between not direct connected layers in a chain of heterogeneous layers in the form of multiplex networks is a challenging problem and is still remains open, best of our knowledge.

In this manuscript, we study the RIS in a chain of layers in the form of a multiplex network. In this RIS, the local dynamics of the nodes in the symmetric position layers (with respect to central layer(s)) which are not directly connected are synchronised due to the signal transfer through relay or intermediate layers, while nodes in each layer do not necessarily synchronised. Here, the symmetric position layers are identical and an impurity in terms of parameter mismatch in the local dynamics of the nodes in the relay layer is introduced. Analytically we derive the invariance or existence condition and then we analyze the local and global stability conditions for the RIS state. We derive the variational equation transverse to the RIS manifold and find the necessary local stability condition using maximum Lyapunov exponent (MLE) of the variational equation. We also derive a global stability condition using Lyapunov function approach.

We study the effect of impurity introduced in the local dynamics of the middle layer on the RIS. The obtained results show that by introducing an impurity in the middle layer, the synchronisation state enhances between symmetric position layers. We discover that the presence of parameter mismatch in the middle layer's local dynamics create a time lag between symmetric position layers and middle layer. This time lag plays an important role in the enhancing of RIS among the symmetric positions layers in the multiplex network. Further, we inspect its robustness against a progressive demultiplexing of the multiplex network structure. For this, we derive an appropriate demultiplexing process so that the RIS solution remains an invariant solution. We analytically derive variational equation transverse to the RIS manifold for the demultiplexed systems. We verify our analytical results by numerical experiments on three and five layers multiplex networks where paradigmatic chaotic systems are used as the local dynamics of the node.

2. Mathematical preliminaries

This section illustrates some background knowledge related to this work, especially on the basic of graph theory. A complex network or a graph is a pair $G = (V, E)$, where V is the set of vertices and E denotes the set of edges connecting the vertices. Various type of interactions are found to systematically organise different classes of complex network architectures. A multiplex network is one of the network architecture and represented as a pair $\mathcal{M} = (\mathcal{G}, \mathcal{C})$, where $\mathcal{G} = \{\mathcal{G}_\alpha = (V_\alpha, E_\alpha) : \alpha = 1, 2, \dots, Q\}$ is a family of networks and Q is the number of layers. Here, N is the number of nodes in each layer G_α , i.e., $|V_1| = |V_2| = \dots = |V_Q| = N$ and the elements of E_α are called as intralayer connections. $\mathcal{C} = \left\{ \left(v_i^{[\alpha]}, v_i^{[\beta]} \right) : v_i^{[\alpha]} \in V_\alpha, v_i^{[\beta]} \in V_\beta, i = 1, 2, \dots, N; \alpha, \beta = 1, 2, \dots, Q \text{ and } \alpha \neq \beta \right\}$ is the set of edges depicting the interconnections between the nodes of non-identical layers, termed as interlayer connections.

Some necessary notations are used in this manuscript. We endow with the Euclidean norm $\|\mathbf{x}\| = \sqrt{\sum_{i=1}^d x_i^2}$. I_d denotes the identity matrix of order d and Jf is the Jacobian matrix of the function f with respect to its state variable, i.e., $Jf(\mathbf{x}_0, \alpha) = \frac{\partial f(\mathbf{x}, \alpha)}{\partial \mathbf{x}} \Big|_{\mathbf{x}=\mathbf{x}_0}$. For a square matrix A , A^T denotes the transpose of the matrix A and A^* denote its Hermitian. $O_{p \times q}$ denotes the zero matrix of order $p \times q$. $\lambda_{\min}(A)$ denotes the smallest eigenvalue of the matrix A . The matrix Kronecker product and matrix direct sum are denoted by \otimes and \oplus , respectively. For square matrices A and B of same size, few standard properties of the Kronecker product are [47]:

- (a) $(A \otimes B)(C \otimes D) = (AC) \otimes (BD)$,
- (b) $(A \otimes B)^T = A^T \otimes B^T$,
- (c) $(A \otimes B)^{-1} = A^{-1} \otimes B^{-1}$, provided both the matrices A and B are invertible.

3. Mathematical model

We consider a chain of $(2L + 1)$ number of layers in the form of a multiplex network, where the intermediate layers are connected to its nearest layers on both sides and the outermost layers are connected to their nearest layer only. Here L is the number of layers on both sides of the central layer. It is supposed that the local dynamics of the nodes in the symmetric positions layers on both sides with respect to the middlemost layer are identical. Each layer is composed with N nodes of d -dimensional dynamical systems. Figure 1 depicts a schematic diagram of the five-layer (i.e., $L = 2$) multiplex network where the local dynamics of the nodes at the symmetric positions layers, i.e., layer- (± 1) and layer- (± 2) are identical. However, the middlemost layer (blue nodes) acts as a relay layer and the local dynamics of the nodes possess a different parameter value. The dashed black horizontal lines represent the interlayer links between the layers. The intralayer connections in the symmetric positions layers are identical, while the intralayer connections in the central layer is different from the other four layers (in the next section, we will prove it).

Now, the d -dimensional dynamical system is associated with the i th node in the l th layer, whose state is represented by the vector $\mathbf{x}_{l,i}(t) \in \mathbb{R}^d$. Then the mathematical form of the chain of multiplex network can be written as,

$$\dot{\mathbf{x}}_{-L,i} = f(\mathbf{x}_{-L,i}, \alpha_L) + \epsilon \sum_{j=1}^N \mathcal{A}_{ij}^{[-L]} G[\mathbf{x}_{-L,j} - \mathbf{x}_{-L,i}] + \eta H[\mathbf{x}_{-L+1,i} - \mathbf{x}_{-L,i}], \quad (1a)$$

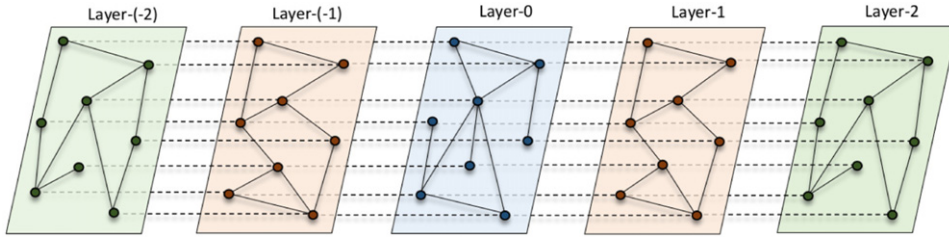


Figure 1. Schematic representation of a five-layer multiplex network with identical oscillators in the two pairs of symmetric positions layers (layer- (± 1) and layer- (± 2)) with respect to the center layer (layer-0). Impurity in terms of parameter mismatch is introduced in the local dynamics of the nodes in the middlemost layer-0. The intralayer networks of the symmetric positions layers are identically drawn (the reason behind this choice is described in lemma 3).

$$\begin{aligned} \dot{\mathbf{x}}_{l,i} = & f(\mathbf{x}_{l,i}, \alpha_{|l|}) + \epsilon \sum_{j=1}^N \mathcal{A}_{ij}^{[l]} G[\mathbf{x}_{l,j} - \mathbf{x}_{l,i}] \\ & + \eta H[\mathbf{x}_{l+1,i} + \mathbf{x}_{l-1,i} - 2\mathbf{x}_{l,i}], \quad l = 0, \pm 1, \pm 2, \dots, \pm(L-1), \end{aligned} \quad (1b)$$

$$\dot{\mathbf{x}}_{L,i} = f(\mathbf{x}_{L,i}, \alpha_L) + \epsilon \sum_{j=1}^N \mathcal{A}_{ij}^{[L]} G[\mathbf{x}_{L,j} - \mathbf{x}_{L,i}] + \eta H[\mathbf{x}_{L-1,i} - \mathbf{x}_{L,i}], \quad (1c)$$

where $i = 1, 2, \dots, N$ is the oscillator index in each layer and the over-dot represents time-derivative. The dynamics of each individual oscillator is governed by the evolution function $f: \mathbb{R}^d \times \mathbb{R} \rightarrow \mathbb{R}^d$. Since our objective is to study the interlayer synchronisation, the vector field is assumed to be identical for each nodes in a particular layer. The interlayer inner-coupling matrix H determines the state variables through which a node of a layer is interacting with its counterpart nodes in the adjacent layers. G is the intralayer inner-coupling matrix which gives the connection of the oscillators within the layer. ϵ is the intralayer coupling strength which controls the interaction between the nodes within a layer. The strength of information convey between the layers is determined by the parameter η , called the interlayer coupling strength. In this multiplex network, $\alpha_{|l|}$ is the system parameter of the layer- l , i.e., the oscillators at the symmetric positions layers have identical parameter values. These symmetric positions layers are indirectly interacting through the intermediate layers. Here, $|l|$ denotes the absolute value of l .

The intralayer network configuration of the layer- l ($l = 0, \pm 1, \pm 2, \dots, \pm L$) corresponding to the graph (V_l, E_l) is encoded by the adjacency matrix $\mathcal{A}^{[l]}$ of order N . Here $\mathcal{A}_{ij}^{[l]} = 1$ if $(v_i^{[l]}, v_j^{[l]}) \in E_l$, i.e., if the i th node and j th node of the layer- l are connected and zero otherwise. $\mathcal{L}^{[l]}$ denotes the corresponding zero-row sum Laplacian matrix and is obtained from the adjacency matrix $\mathcal{A}^{[l]}$. It reads as $\mathcal{L}_{ij}^{[l]} = -\mathcal{A}_{ij}^{[l]}$ if $i \neq j$, and $\mathcal{L}_{ii}^{[l]} = \sum_{j=1}^N \mathcal{A}_{ij}^{[l]}$, i.e., the off-diagonal elements are the negative of the corresponding elements in $\mathcal{A}^{[l]}$ and the diagonal element $\mathcal{L}_{ii}^{[l]}$ is the sum of the non-diagonal elements in the i th row of $\mathcal{A}^{[l]}$. The diagonal matrix $\Lambda^{[l]} = \text{diag}\{0 = \gamma_1^{[l]}, \gamma_2^{[l]}, \dots, \gamma_N^{[l]}\}$ consists of the eigenvalues of $\mathcal{L}^{[l]}$. Here, we rigorously analyze the existence and stability conditions of the RIS state in this proposed multiplex network architecture.

4. Analytical results

Interlayer synchronisation state occurs in the multiplex network (3) if each node in a given layer evolves synchronously with its replica nodes in the other layers, regardless of whether it is synchronised with the other nodes of the same layer. Mathematically, we can write, $\|\mathbf{x}_{k,i}(t) - \mathbf{x}_{l,i}(t)\| \rightarrow 0$ as $t \rightarrow \infty$ for all $i = 1, 2, \dots, N$; $k, l \in \{0, \pm 1, \pm 2, \dots, \pm L\}$ and $k \neq l$.

First we check whether the interlayer synchronisation state will be an invariant solution for the multiplex network (3) or not. Then, under the invariance condition, we analytically derive the local and global stability conditions for the RIS state. Finally, we proposed an appropriate demultiplexing process and derive the variational equation transverse to the RIS manifold for demultiplex network.

4.1. Invariance of interlayer synchronisation

The following lemma illustrates the invariance of the RIS state.

Lemma 1. *The interlayer synchronisation solution is not an invariant solution for the multiplex network (3), whatever be the intralayer and interlayer coupling strengths.*

Proof of Lemma 1. See appendix A.1. \square

The parameter mismatch in the nodal dynamics of the layers gives a non-invariance of the interlayer synchronisation state in the system (3) for $(2L + 1)$ layers. However, the replica-wise interlayer synchronisation may be possible between the symmetric positions layers. The RIS state is defined as the interlayer synchronisation between symmetric positions layers which are indirectly coupled through the relay layers, regardless of whether it is synchronised with the other nodes of its own layer and its replica nodes in the other non-symmetric positions layers.

Definition 2. The multiplex network (3) is said to achieve the RIS state if for all $l = 1, 2, \dots, L$ and for each node $i = 1, 2, \dots, N$, $\lim_{t \rightarrow \infty} \|\mathbf{x}_{l,i}(t) - \mathbf{x}_{-l,i}(t)\| = 0$.

Thus, each replica nodes of the symmetric positions layers asymptotically converge to each other, regardless of the node dynamics of each individual layers and the replica dynamics of non-symmetric positions layers. The corresponding RIS manifold can be defined as,

$$\mathcal{S}^{\text{RIS}} = \left\{ (\mathbf{x}_{1,1}(t), \mathbf{x}_{1,2}(t), \dots, \mathbf{x}_{L,N-1}(t), \mathbf{x}_{L,N}(t)) \right. \\ \left. \subset \mathbb{R}^{dNL} : \mathbf{x}_{l,i}(t) = \mathbf{x}_{-l,i}(t), \forall i = 1, 2, \dots, N \text{ and } l = 1, 2, \dots, L \right\}. \quad (2)$$

The stabilisation of this manifold \mathcal{S}^{RIS} gives the stability of the RIS solution. If this manifold is stable with respect to the perturbation in its transverse subspace, then the RIS state can be observed. The following lemma gives the invariant nature of \mathcal{S}^{RIS} for the multiplex network (3).

Lemma 3. *The RIS state for the multiplex network (3) will be an invariant solution if the intralayer network architectures of the symmetric positions layers are identical. In other words $\mathcal{L}^{[l]} = \mathcal{L}^{[-l]}$ for all $l = 1, 2, \dots, L$.*

Proof of Lemma 3. See appendix A.2. \square

Thus, with respect to the innermost layer, the intralayer network configurations in symmetric positions layers should be identical for the invariance of the RIS state in the multiplex network (3). Henceforth, we will denote the common Laplacian matrix for the layers- $(\pm l)$ by $\mathcal{L}^{[l]}$ and the corresponding adjacency matrix will be denoted by $\mathcal{A}^{[l]}$. Then the evolution of the manifold \mathcal{S}^{RIS} is governed by the equations

$$\begin{aligned}\dot{\mathbf{x}}_{l,i} &= f(\mathbf{x}_{l,i}, \alpha_l) + \epsilon \sum_{j=1}^N \mathcal{A}_{ij}^{[l]} G[\mathbf{x}_{l,j} - \mathbf{x}_{l,i}] + \eta H[\mathbf{x}_{l+1,i} + \mathbf{x}_{l-1,i} - 2\mathbf{x}_{l,i}], \quad l = 1, 2, \dots, L-1, \\ \dot{\mathbf{x}}_{L,i} &= f(\mathbf{x}_{L,i}, \alpha_L) + \epsilon \sum_{j=1}^N \mathcal{A}_{ij}^{[L]} G[\mathbf{x}_{L,j} - \mathbf{x}_{L,i}] + \eta H[\mathbf{x}_{L-1,i} - \mathbf{x}_{L,i}],\end{aligned}\quad (3)$$

where the reference state variables $\mathbf{x}_{0,i}$ of the i th node ($i = 1, 2, \dots, N$) in the layer-0 (central layer) satisfy the equation of motion,

$$\dot{\mathbf{x}}_{0,i} = f(\mathbf{x}_{0,i}, \alpha_0) + \epsilon \sum_{j=1}^N \mathcal{A}_{ij}^{[0]} G[\mathbf{x}_{0,j} - \mathbf{x}_{0,i}] + \eta H[\mathbf{x}_{1,i} + \mathbf{x}_{-1,i} - 2\mathbf{x}_{0,i}]. \quad (4)$$

Now a central question arising from the dynamical system point of view is about its stability. The local and global stability of \mathcal{S}^{RIS} can be determined as a function of the intralayer and interlayer coupling strengths, and the spectral properties of the intralayer Laplacian matrices. For the RIS state, complete interlayer synchronisation occurs between each replica nodes in the symmetric position layers. In absence of the interlayer coupling, i.e., $\eta = 0$, the replica node dynamics are desynchronised due to the uncoupled layers. By gradually increasing the values of η , a transition from desynchronisation to synchronisation occurs among the replica nodes of the symmetric position layers. Now we explore how the interlayer synchronisation occurs between the symmetric positions layers simultaneously.

Lemma 4. *For the multiplex network (3), the interlayer synchronisations of the symmetric position layers occur simultaneously with respect to the interlayer coupling strength η .*

Proof of Lemma 4. See appendix A.3. \square

To understand the mechanism of the RIS state, it was essential to understand the intralayer network configurations which we have discussed above. Next, we devote our attention on the investigation for the stability of RIS state in the multiplex network (3). By using the eigenvalue analysis, next we analytically derive the local stability using the master stability function approach [48] and global stability criteria by constructing a suitable Lyapunov function for such synchronisation states.

4.2. Stability of relay interlayer synchronisation state

Considering the invariance condition of the RIS state, the equation of motion of our considered multiplex network becomes,

$$\dot{\mathbf{x}}_{-L,i} = f(\mathbf{x}_{-L,i}, \alpha_L) + \epsilon \sum_{j=1}^N \mathcal{A}_{ij}^{[L]} G[\mathbf{x}_{-L,j} - \mathbf{x}_{-L,i}] + \eta H[\mathbf{x}_{-L+1,i} - \mathbf{x}_{-L,i}], \quad (5a)$$

$$\begin{aligned}\dot{\mathbf{x}}_{l,i} &= f(\mathbf{x}_{l,i}, \alpha_{|l|}) + \epsilon \sum_{j=1}^N \mathcal{A}_{ij}^{[|l|]} G[\mathbf{x}_{l,j} - \mathbf{x}_{l,i}] \\ &\quad + \eta H[\mathbf{x}_{l+1,i} + \mathbf{x}_{l-1,i} - 2\mathbf{x}_{l,i}], \quad l = 0, \pm 1, \pm 2, \dots, \pm(L-1),\end{aligned}\quad (5b)$$

$$\dot{\mathbf{x}}_{L,i} = f(\mathbf{x}_{L,i}, \alpha_L) + \epsilon \sum_{j=1}^N \mathcal{A}_{ij}^{[L]} G[\mathbf{x}_{L,j} - \mathbf{x}_{L,i}] + \eta H[\mathbf{x}_{L-1,i} - \mathbf{x}_{L,i}], \quad (5c)$$

where $i = 1, 2, \dots, N$. For the purpose of local stability criterion, we need the following assumption on the local dynamics of each isolated node.

Assumption 5. The individual nodal dynamics $f: \mathbb{R}^d \times \mathbb{R} \rightarrow \mathbb{R}^d$ is continuously differentiable with respect to its first argument.

This assumption ensures the existence of the Jacobian matrix of the vector field f with respect to its first argument.

For the pair of symmetric positions layers $\pm l$, consider the perturbations of its i th replica nodes from the manifold \mathcal{S}^{RIS} as $\delta \mathbf{x}_{l,i}(t)$ for all $i = 1, 2, \dots, N$. The next theorem gives the variational equation transverse to the manifold \mathcal{S}^{RIS} .

Theorem 6. If $\delta \mathbf{x}_l(t)$ denotes the stack of perturbations $\delta \mathbf{x}_{l,1}(t), \delta \mathbf{x}_{l,2}(t), \dots, \delta \mathbf{x}_{l,N}(t)$, then the error components transverse to \mathcal{S}^{RIS} satisfy the evolution equation,

$$\begin{aligned} \delta \dot{\mathbf{x}}_1(t) &= \left[\bigoplus_{i=1}^N Jf(\mathbf{x}_{1,i}, \alpha_1) - \epsilon \mathcal{L}^{[1]} \otimes G \right] \delta \mathbf{x}_1 + \eta I_N \otimes H[\delta \mathbf{x}_2 - \delta \mathbf{x}_1], \\ \delta \dot{\mathbf{x}}_l(t) &= \left[\bigoplus_{i=1}^N Jf(\mathbf{x}_{l,i}, \alpha_l) - \epsilon \mathcal{L}^{[l]} \otimes G \right] \delta \mathbf{x}_l + \eta I_N \otimes H[\delta \mathbf{x}_{l+1} + \delta \mathbf{x}_{l-1} - 2\delta \mathbf{x}_l], \\ &\quad l = 2, 3, \dots, L-1, \\ \delta \dot{\mathbf{x}}_L(t) &= \left[\bigoplus_{i=1}^N Jf(\mathbf{x}_{L,i}, \alpha_L) - \epsilon \mathcal{L}^{[L]} \otimes G \right] \delta \mathbf{x}_L + \eta I_N \otimes H[\delta \mathbf{x}_{L-1} - \delta \mathbf{x}_L]. \end{aligned} \quad (6)$$

Here, $(\mathbf{x}_{l,1}, \mathbf{x}_{l,2}, \dots, \mathbf{x}_{l,N} : l = 1, 2, \dots, L)$ is the state variable of the RIS solution satisfying equation (3).

Proof of Theorem 6. If the RIS emerges in the multiplex network (5), then for all l and i , $\mathbf{x}_{l,i}(t) = \mathbf{x}_{-l,i}(t)$ as $t \rightarrow \infty$. Consider each node of the layer- $(-l)$ as reference trajectory. If $\delta \mathbf{x}_{l,i}(t)$ denotes the perturbation of the i th node in the layer- l from \mathcal{S}^{RIS} , then we can write the present state variable of this node as $\mathbf{x}_{l,i}(t) = \mathbf{x}_{-l,i}(t) + \delta \mathbf{x}_{l,i}(t)$. Then, the rate of change of the perturbation term $\delta \mathbf{x}_{l,i}(t)$ is $\delta \dot{\mathbf{x}}_{l,i}(t) = \dot{\mathbf{x}}_{l,i}(t) - \dot{\mathbf{x}}_{-l,i}(t)$ for $l = 1, 2, \dots, L$.

Considering small perturbations from \mathcal{S}^{RIS} and expanding the vector field f in the Taylor series expansion up to the first order, we can write

$$\begin{aligned} \delta \dot{\mathbf{x}}_{1,i}(t) &= Jf(\mathbf{x}_{1,i}, \alpha_1) \delta \mathbf{x}_{1,i} + \epsilon \sum_{j=1}^N \mathcal{A}_{ij}^{[1]} G[\delta \mathbf{x}_{1,j} - \delta \mathbf{x}_{1,i}] + \eta H[\delta \mathbf{x}_{2,i} - \delta \mathbf{x}_{1,i}], \\ \delta \dot{\mathbf{x}}_{l,i}(t) &= Jf(\mathbf{x}_{l,i}, \alpha_l) \delta \mathbf{x}_{l,i} + \epsilon \sum_{j=1}^N \mathcal{A}_{ij}^{[l]} G[\delta \mathbf{x}_{l,j} - \delta \mathbf{x}_{l,i}] \\ &\quad + \eta H[\delta \mathbf{x}_{l+1,i} + \delta \mathbf{x}_{l-1,i} - 2\delta \mathbf{x}_{l,i}], \quad l = 2, 3, \dots, L-1, \\ \delta \dot{\mathbf{x}}_{L,i}(t) &= Jf(\mathbf{x}_{L,i}, \alpha_L) \delta \mathbf{x}_{L,i} + \epsilon \sum_{j=1}^N \mathcal{A}_{ij}^{[L]} G[\delta \mathbf{x}_{L,j} - \delta \mathbf{x}_{L,i}] + \eta H[\delta \mathbf{x}_{L-1,i} - \delta \mathbf{x}_{L,i}]. \end{aligned} \quad (7)$$

In the vectorial form, the above error equations can be written as equation (6). \square

In our case, Lyapunov exponent measures the exponential contraction or expansion rate of an infinitesimal perturbations of the error system (6). The Lyapunov exponents can be ascertained by the linearised equation (6) with respect to the reference trajectories satisfying equations (3) and (4). Among all the Lyapunov exponents Λ_j ($j = 1, 2, \dots, 3N$) of equation (6), the largest one called as MLE and denoted by Λ_{\max} . It plays a key role for the stability of the RIS state. For desynchronised motions of each replica node among the two outer layers, where the individual oscillators are chaotic, the error state variable $\delta \mathbf{x}(t)$ evolves chaotically. So for that case, Λ_{\max} will be greater than zero. By tuning the coupling strengths and network parameters if the RIS state occurs then $\delta \mathbf{x}(t) \rightarrow 0$ as $t \rightarrow \infty$. Due to the stabilisation of system equation (6) at that parameter values, Λ_{\max} becomes negative. The maximum of the Lyapunov exponent as a function of the parameters $(\epsilon, \eta, \Delta\omega)$ gives the necessary condition for the local stability of the RIS state. Whenever $\Lambda_{\max} < 0$, the perturbations transverse to that manifold die out, and all the replicas corresponding to the layer- l and layer- $(-l)$ evolve coherently. So the negativity of the Λ_{\max} obtained from the linearised equation (6) together with equations (3) and (4) implies stable RIS state.

However, the above linear stability analysis reflects only local stability of the synchronisation states. It is valid only for infinitesimally small perturbations around the RIS manifold, thus failing to characterise the stability against significantly large perturbations. When studying synchronisation states, a central problem is to find suitable conditions that ensure global stability of all dynamical oscillators toward the synchronisation manifold \mathcal{S}^{RIS} . Next, we derive the global stability condition of this synchronisation state, which secures the stability of each replica nodes between the symmetric positions layers to a common trajectory irrespective of any initial conditions. To derive the global stability condition of the RIS state, we need the following assumptions on the dynamics of each isolated node, intralayer and interlayer coupling functions and topologies of the intralayer connections.

Assumption 7. The isolated evolution function $f: \mathbb{R}^d \times \mathbb{R} \rightarrow \mathbb{R}^d$ satisfies a global Lipschitz condition, i.e., there exist non-negative constant M_α such that for any two vectors $\mathbf{x}, \mathbf{y} \in \mathbb{R}^d$, we have

$$\|f(\mathbf{x}, \alpha) - f(\mathbf{y}, \alpha)\| \leq M_\alpha \|\mathbf{x} - \mathbf{y}\|. \quad (8)$$

This ensures the upper bound of the rate of change of individual node dynamics in its phase space.

Assumption 8. The intralayer Laplacian matrix $\mathcal{L}^{[l]}$ is symmetric for all l ($l = 1, 2, \dots, L$), i.e., the intralayer network in the layer- l is bidirectional. So $\mathcal{L}^{[l]}$ is a symmetric positive semi-definite matrix. We can sort the associated eigenvalues of $\mathcal{L}^{[l]}$ as $0 = \gamma_1^{[l]} < \gamma_2^{[l]} \leq \dots \leq \gamma_N^{[l]}$.

This assumption assures us that all eigenvalues of $\mathcal{L}^{[l]}$ are real, moreover, it is a positive semi-definite matrix with one zero eigenvalue.

Assumption 9. The interlayer coupling matrix H is symmetric positive definite. Then, we can sort its eigenvalues as $0 < \mu_1 \leq \mu_2 \leq \dots \leq \mu_d$.

This assumption ensures that all the eigenvalues of H are positive.

Assumption 10. The intralayer coupling matrix G is a symmetric positive semi-definite. Therefore, all its eigenvalues are non-negative.

Proposition 11. *If A is a real symmetric matrix of order N with sorted eigenvalues $\lambda_1 \leq \lambda_2 \leq \dots \leq \lambda_N$, then*

$$\lambda_1 \mathbf{x}^{\text{tr}} \mathbf{x} \leq \mathbf{x}^{\text{tr}} A \mathbf{x} \leq \lambda_N \mathbf{x}^{\text{tr}} \mathbf{x}.$$

This proposition gives the bound of the quadratic form $\mathbf{x}^{\text{tr}} A \mathbf{x}$.

Proposition 12. *Let A be a symmetric positive semi-definite matrix of order n . Then, for any $\mathbf{x}, \mathbf{y} \in \mathbb{R}^n$, A satisfies the condition $\mathbf{x}^{\text{tr}} A \mathbf{y} \leq \frac{1}{2}[\mathbf{x}^{\text{tr}} A \mathbf{x} + \mathbf{y}^{\text{tr}} A \mathbf{y}]$.*

The above two propositions are well-known in linear algebra and will be used in the global stability analysis.

Theorem 13. *Given a multiplex network (5) of three layers, i.e., $L = 1$, and N nodes in each layer. Consider that the isolate node dynamics of the multiplex network satisfies the assumption 7, the intralayer Laplacian matrix satisfies the assumption 8, the intralayer and the interlayer inner-coupling matrices respectively satisfy the assumptions 9 and 10. Then, the RIS state of this multiplex network will be globally stable if $\eta > \frac{M}{\mu_1}$.*

Proof of Theorem 13. The global stability condition will be derived in terms of the convergence properties of the trajectory of each node in the layer- l associated to the trajectory of its counter part node in the layer- $(-l)$ for non-local perturbation from manifold S^{RIS} . Let $\delta \mathbf{x}_{l,i}(t)$ be the interlayer synchronisation error term of the i th replica node between the symmetric position layers- $(\pm l)$ and defined as $\delta \mathbf{x}_{l,i}(t) = \mathbf{x}_{l,i}(t) - \mathbf{x}_{-l,i}(t)$.

Now, we define a Lyapunov function in terms of the error quantities as,

$$V(t) = \frac{1}{2} \sum_{l=1}^L \delta \mathbf{x}_l^{\text{tr}}(t) \delta \mathbf{x}_l(t), \quad (9)$$

where $\delta \mathbf{x}_l(t)$ is the stack of the error terms $\delta \mathbf{x}_{l,1}(t), \delta \mathbf{x}_{l,2}(t), \dots, \delta \mathbf{x}_{l,N}(t)$. The time derivative of $V(t)$ along the RIS solution can be written as,

$$\begin{aligned} \dot{V}(t) &= \sum_{l=1}^L \sum_{i=1}^N \delta \mathbf{x}_{l,i}^{\text{tr}}(t) \delta \dot{\mathbf{x}}_{l,i}(t) = \sum_{l=1}^L \sum_{i=1}^N \delta \mathbf{x}_{l,i}^{\text{tr}} [f(\mathbf{x}_{l,i}, \alpha_l) - f(\mathbf{x}_{-l,i}, \alpha_l)] \\ &\quad - \epsilon \sum_{l=1}^L \sum_{i=1}^N \sum_{j=1}^N \delta \mathbf{x}_{l,i}^{\text{tr}} \mathcal{L}_{ij}^{[l]} G \delta \mathbf{x}_{l,j} + \eta \sum_{i=1}^N \delta \mathbf{x}_{1,i}^{\text{tr}} H[\delta \mathbf{x}_{2,i} - 2\delta \mathbf{x}_{1,i}] \\ &\quad + \eta \sum_{l=2}^{L-1} \sum_{i=1}^N \delta \mathbf{x}_{l,i}^{\text{tr}} H[\delta \mathbf{x}_{l+1,i} + \delta \mathbf{x}_{l-1,i} - 2\delta \mathbf{x}_{l,i}] \\ &\quad + \eta \sum_{i=1}^N \delta \mathbf{x}_{L,i}^{\text{tr}} H[\delta \mathbf{x}_{L-1,i} - \delta \mathbf{x}_{L,i}]. \end{aligned} \quad (10)$$

By using the Cauchy–Schwartz inequality and the Lipschitz property of the nodal dynamics f , for all $\mathbf{x}, \mathbf{y} \in \mathbb{R}^d$, we have,

$$\begin{aligned} [\mathbf{x} - \mathbf{y}]^{\text{tr}} [f(\mathbf{x}, \alpha_l) - f(\mathbf{y}, \alpha_l)] &\leq \|\mathbf{x} - \mathbf{y}\| \|f(\mathbf{x}, \alpha_l) - f(\mathbf{y}, \alpha_l)\| \\ &\leq M_l [\mathbf{x} - \mathbf{y}]^{\text{tr}} [\mathbf{x} - \mathbf{y}], \end{aligned} \quad (11)$$

where $l = 1, 2, \dots, L$. Here, M_l is the Lipschitz constant of the vector field f with respect to its second argument α_l .

Using the above inequality in the equation (10), for any vectors $\mathbf{x}_{l,i} \in \mathbb{R}^d$, we get an upper bound of $\dot{V}(t)$ as,

$$\begin{aligned} \dot{V}(t) \leq & \sum_{l=1}^L \sum_{i=1}^N \delta \mathbf{x}_{l,i}^{\text{tr}} M_l \delta \mathbf{x}_{l,i} - \epsilon \sum_{l=1}^L \sum_{i=1}^N \sum_{j=1}^N \delta \mathbf{x}_{l,i}^{\text{tr}} \mathcal{L}_{ij}^{[l]} G \delta \mathbf{x}_{l,j} \\ & + \eta \sum_{i=1}^N \delta \mathbf{x}_{1,i}^{\text{tr}} H [\delta \mathbf{x}_{2,i} - 2\delta \mathbf{x}_{1,i}] + \eta \sum_{l=2}^{L-1} \sum_{i=1}^N \delta \mathbf{x}_{l,i}^{\text{tr}} H [\delta \mathbf{x}_{l+1,i} + \delta \mathbf{x}_{l-1,i} - 2\delta \mathbf{x}_{l,i}] \\ & + \eta \sum_{i=1}^N \delta \mathbf{x}_{L,i}^{\text{tr}} H [\delta \mathbf{x}_{L-1,i} - \delta \mathbf{x}_{L,i}]. \end{aligned} \quad (12)$$

Now, using proposition 12, we can write

$$\begin{aligned} & \sum_{i=1}^N \delta \mathbf{x}_{1,i}^{\text{tr}} H \delta \mathbf{x}_{2,i} + \sum_{l=2}^{L-1} \sum_{i=1}^N \delta \mathbf{x}_{l,i}^{\text{tr}} H [\delta \mathbf{x}_{l+1,i} + \delta \mathbf{x}_{l-1,i}] + \sum_{i=1}^N \delta \mathbf{x}_{L,i}^{\text{tr}} H \delta \mathbf{x}_{L-1,i} \\ & \leq \sum_{i=1}^N \delta \mathbf{x}_{1,i}^{\text{tr}} H \delta \mathbf{x}_{1,i} + 2 \sum_{l=2}^{L-1} \sum_{i=1}^N \delta \mathbf{x}_{l,i}^{\text{tr}} H \delta \mathbf{x}_{l,i} + \sum_{i=1}^N \delta \mathbf{x}_{L,i}^{\text{tr}} H \delta \mathbf{x}_{L,i}. \end{aligned} \quad (13)$$

Then the inequality (12) becomes,

$$\dot{V}(t) \leq \sum_{l=1}^L \sum_{i=1}^N \delta \mathbf{x}_{l,i}^{\text{tr}} M_l \delta \mathbf{x}_{l,i} - \epsilon \sum_{l=1}^L \sum_{i=1}^N \sum_{j=1}^N \delta \mathbf{x}_{l,i}^{\text{tr}} \mathcal{L}_{ij}^{[l]} G \delta \mathbf{x}_{l,j} - \eta \sum_{i=1}^N \delta \mathbf{x}_{1,i}^{\text{tr}} H \delta \mathbf{x}_{1,i}. \quad (14)$$

In vectorial form, the above inequality can be written as,

$$\dot{V}(t) \leq \sum_{l=1}^L M_l \delta \mathbf{x}_l^{\text{tr}} \delta \mathbf{x}_l - \epsilon \sum_{l=1}^L \delta \mathbf{x}_l^{\text{tr}} [\mathcal{L}^{[l]} \otimes G] \delta \mathbf{x}_l - \eta \delta \mathbf{x}_1^{\text{tr}} [I_N \otimes H] \delta \mathbf{x}_1. \quad (15)$$

Now, applying proposition 11, we can write,

$$\dot{V}(t) \leq \sum_{l=1}^L M_l \delta \mathbf{x}_l^{\text{tr}} \delta \mathbf{x}_l - \epsilon \sum_{l=1}^L \delta \mathbf{x}_l^{\text{tr}} \lambda_{\min}(\mathcal{L}^{[l]} \otimes G) \delta \mathbf{x}_l - \eta \delta \mathbf{x}_1^{\text{tr}} \lambda_{\min}(I_N \otimes H) \delta \mathbf{x}_1. \quad (16)$$

Since, for all $l = 1, 2, \dots, L$, the smallest eigenvalue of $\mathcal{L}^{[l]}$ is zero, G is a positive semi-definite matrix. Therefore, we have $\lambda_{\min}(\mathcal{L}^{[l]} \otimes G) = \lambda_{\min}(\mathcal{L}^{[l]}) \lambda_{\min}(G) = 0$. Similarly, as the smallest eigenvalues of H is μ_1 , therefore $\lambda_{\min}(I_N \otimes H) = \mu_1$.

Additionally, assuming $M = \max\{M_l : l = 1, 2, \dots, L\}$, we have

$$\dot{V}(t) \leq M \sum_{l=1}^L \delta \mathbf{x}_l^{\text{tr}} \delta \mathbf{x}_l - \eta \mu_1 \delta \mathbf{x}_1^{\text{tr}} \delta \mathbf{x}_1. \quad (17)$$

Since $L = 1$ for triplex network, therefore towards the negative definiteness of $\dot{V}(t)$, it is sufficient to have $\eta > \frac{M}{\mu_1}$. This is our required global stability condition. \square

This result depicts that the critical interlayer coupling strength for global stability is inversely proportional to the smallest eigenvalue of the interlayer inner-coupling matrix H .

In this global stability analysis, we are interested in finding conditions for the global convergence of all dynamical oscillators toward the synchronisation manifold \mathcal{S}^{RIS} irrespective of any initial conditions from its phase space. When studying synchronisation states, a crucial problem is to find such conditions. Construction of different Lyapunov function may improve the required critical coupling strength for the global stability of the RIS state.

To derive the global stability condition, we have adopted the Lyapunov-based method by constructing a quadratic Lyapunov function under few mild assumptions. This method provides a sufficient condition for the global stability, but not a necessary condition. Therefore, the required coupling strength obtained from this approach is usually far away from the exact critical coupling strength for global stability. However, one can construct more suitable Lyapunov functions to optimise the global stability condition. For such purpose, the Lyapunov optimisation technique [49–52] could be an appropriate tool, which refers to the use of Lyapunov function to optimally control a dynamical system.

4.3. Demultiplexing effect

RIS is an emerging process of multiplex networks with $(2L + 1)$ number of layers, whereby each node in a layer evolves synchronously with its replica nodes in the symmetric positions layer, irrespective of whether it is synchronised with the replica nodes in the other layers. Now, we investigate the robustness of the RIS against progressive demultiplexing of the replica (interlayer) connections in the multiplex network (3). The effect of demultiplexing on the interlayer synchronisation in a two-layer multiplex network has been numerically investigated in references [24, 26]. In our multiplex network, there are total $2LN$ number of interlayer connections. We can remove interlayer connections between any two adjacent layers. Therefore, in this multiplex network, we can remove replica connections in $2^{2LN} - 1$ different ways.

Consider an array $\mathbf{b}_{k+1,k}$ of size $N \times 1$, which encodes the multiplexing of interlayer connections among layer- k and layer- $(k + 1)$ for $k = 0, \pm 1, \pm 2, \dots, \pm(L - 1), \pm L$. This array is defined as

$$\begin{aligned} \mathbf{b}_{k+1,k}(i) &= 1, \quad \text{if the } i\text{th replica nodes of the } (k + 1)\text{th and } k\text{th layers are connected,} \\ &= 0, \quad \text{otherwise.} \end{aligned} \quad (18)$$

By considering this progressive demultiplexing, the interlayer coupling terms (3rd term in the right-hand side) of equations (5a)–(5c) will be replaced by $\eta \mathbf{b}_{L,L-1}(i)H(\mathbf{x}_{L-1,i} - \mathbf{x}_{L,i})$, $\eta [\mathbf{b}_{l+1,l}(i)H(\mathbf{x}_{l+1,i} - \mathbf{x}_{l,i}) + \mathbf{b}_{l,l-1}(i)H(\mathbf{x}_{l-1,i} - \mathbf{x}_{l,i})]$, and $\eta \mathbf{b}_{-L+1,-L}(i)H(\mathbf{x}_{-L+1,i} - \mathbf{x}_{-L,i})$, respectively. Since, we are considering bidirectional interlayer connections, therefore $\mathbf{b}_{l,l-1} = \mathbf{b}_{l-1,l}$ for all l .

Under appropriate demultiplexing of replica connections, the RIS state can be an invariant solution. The following lemma illustrates it in details.

Lemma 14. *If there exists $i_1, i_2, \dots, i_m \in \{1, 2, \dots, N\}$ (where $m < N$) and $k \in \{1, 2, \dots, L\}$ such that*

$$\begin{aligned} \mathbf{b}_{k+1,k}(i) &= \mathbf{b}_{-k,-k-1}(i) = 0, \quad \text{for } i = i_1, i_2, \dots, i_m, \\ &= 1, \quad \text{otherwise.} \end{aligned} \quad (19)$$

Moreover, $\mathbf{b}_{l+1,l}(i) = \mathbf{b}_{-l+1,-l}(i) = 1$ for all $l \neq k$ and i . Then the RIS solution will be an invariant solution.

Proof of Lemma 14. See appendix A.4. □

On the other hand, suppose, there exists $i \in \{1, 2, \dots, N\}$ such that $\mathbf{b}_{l,l-1}(i) = 0$ for some l and all others $\mathbf{b}_{l,l-1}(i) = 1$. For this demultiplexing scheme, if possible, assume that the RIS state is an invariant solution. Then, if the initial condition of the replica-wise state variables of symmetric positions layers are equal, then they persist for further higher time-instances.

Consider at the initial time $t = t_0$, $\mathbf{x}_{l,i}(t_0) = \mathbf{x}_{-l,i}(t_0)$ for $l = 1, 2, \dots, L$. Now the difference between the rate of change of this replica nodes at the symmetric positions layers (l th and $(-l)$ th layers) becomes

$$\dot{\mathbf{x}}_{l,i}(t_0) - \dot{\mathbf{x}}_{-l,i}(t_0) = -\eta H [\mathbf{x}_{-l+1,i}(t_0) - \mathbf{x}_{-l,i}(t_0)] \mathbf{b}_{-l+1,-l}(i). \quad (20)$$

Therefore, it is clear that, $\dot{\mathbf{x}}_{l,i}(t_0) \neq \dot{\mathbf{x}}_{-l,i}(t_0)$. This non-identical rate of change of the two-replica nodes signifies their separate trajectories in the next time instance. Therefore, if we remove an interlayer connection between the i th node in the l th layer and $(l-1)$ th layer, and not remove the corresponding interlayer connection among the symmetric positions layers, i.e., $(-l)$ th layer and $(-l+1)$ th layer, then the RIS becomes not invariant solution. Similarly, the presence of multiple heterogeneous demultiplexing give non-invariance of this synchronisation pattern.

However, by simultaneously demultiplexing these replica connections the RIS could be possible subject to the stability of this state.

Using lemma 14, the manifold \mathcal{S}^{RIS} satisfies the evolution equation,

$$\begin{aligned} \dot{\mathbf{x}}_{l,i} &= f(\mathbf{x}_{l,i}, \alpha_{|l|}) - \epsilon \sum_{j=1}^N \mathcal{L}_{ij}^{[|l|]} G \mathbf{x}_{l,j} + \eta H [\mathbf{b}_{l+1,l}(i)(\mathbf{x}_{l+1,i} - \mathbf{x}_{l,i}) \\ &\quad + \mathbf{b}_{l,l-1}(i)(\mathbf{x}_{l-1,i} - \mathbf{x}_{l,i})], \quad l = 1, 2, \dots, L-1, \\ \dot{\mathbf{x}}_{L,i} &= f(\mathbf{x}_{L,i}, \alpha_L) + \epsilon \sum_{j=1}^N \mathcal{L}_{ij}^{[L]} G [\mathbf{x}_{L,j} - \mathbf{x}_{L,i}] + \eta \mathbf{b}_{L,L-1}(i) H [\mathbf{x}_{L-1,i} - \mathbf{x}_{L,i}], \end{aligned} \quad (21)$$

where $\mathbf{x}_{0,i}$, $i = 1, 2, \dots, N$, are the reference state variables in the middlemost layer, which satisfy the evolution equation,

$$\dot{\mathbf{x}}_{0,i} = f(\mathbf{x}_{0,i}, \alpha_0) + \epsilon \sum_{j=1}^N \mathcal{L}_{ij}^{[0]} G [\mathbf{x}_{0,j} - \mathbf{x}_{0,i}] + 2\eta \mathbf{b}_{1,0}(i) H [\mathbf{x}_{1,i} - \mathbf{x}_{0,i}]. \quad (22)$$

The RIS will be observed physically if it is stable. The local stability analysis for such progressive demultiplexing is given in the next theorem.

Theorem 15. *Due to the systematic demultiplexing of the replica connections (using lemma 14), the error components transverse to the synchronisation manifold \mathcal{S}^{RIS} satisfy the evolution equation,*

$$\begin{aligned} \delta \dot{\mathbf{x}}_1(t) &= \left[\bigoplus_{i=1}^N Jf(\mathbf{x}_{1,i}, \alpha_1) - \epsilon \mathcal{L}^{[1]} \otimes G - \eta (\mathbf{B}_{1,0} + \mathbf{B}_{2,1}) \otimes H \right] \delta \mathbf{x}_1 \\ &\quad + \eta \mathbf{B}_{2,1} \otimes H \delta \mathbf{x}_2, \\ \delta \dot{\mathbf{x}}_l(t) &= \left[\bigoplus_{i=1}^N Jf(\mathbf{x}_{l,i}, \alpha_l) - \epsilon \mathcal{L}^{[l]} \otimes G - \eta (\mathbf{B}_{l,l-1} + \mathbf{B}_{l+1,l}) \otimes H \right] \delta \mathbf{x}_l \\ &\quad + \eta [\mathbf{B}_{l,l-1} \otimes H \delta \mathbf{x}_{l-1} + \mathbf{B}_{l+1,l} \otimes H \delta \mathbf{x}_{l+1}], \quad l = 2, 3, \dots, L-1, \end{aligned}$$

$$\begin{aligned} \delta \dot{\mathbf{x}}_L(t) = & \left[\bigoplus_{i=1}^N Jf(\mathbf{x}_{L,i}, \alpha_L) - \epsilon \mathcal{L}^{[L]} \otimes G - \eta \mathbf{B}_{L,L-1} \otimes H \right] \delta \mathbf{x}_L \\ & + \eta \mathbf{B}_{L,L-1} \otimes H \delta \mathbf{x}_{L-1}, \end{aligned} \quad (23)$$

where $\mathbf{B}_{l+1,l} = \text{diag}(\mathbf{b}_{l+1,l}(1), \mathbf{b}_{l+1,l}(2), \dots, \mathbf{b}_{l+1,l}(N))$.

Proof of Theorem 15. See appendix A.5. \square

Next, we numerically illustrate our theoretical results for multiplex networks consisting of three and five layers.

5. Numerical illustrations for three-layer (i.e., $L = 1$) multiplex networks

To verify the obtained analytical results for the emergence of RIS, we first consider three-layer multiplex networks in which the outer two layers are connected indirectly through the mismatch middle (relay) layer.

We consider two different local dynamics in the nodes: Lorenz and Rössler systems. Each layer of the network has Erdős–Rényi (ER) random structure, consisting of $N = 200$ number of nodes. For the three-layer multiplex network, the RIS occurs when each subsystem in the layer-1 evolves synchronously with its counterpart node in the layer-(-1). Here we delve into this state by changing the coupling strengths and network parameters. In order to evaluate the RIS state, the associated synchronisation error is defined as

$$E^{\text{RIS}} = \lim_{T \rightarrow \infty} \frac{1}{T} \int_{t_r}^{t_r+T} E^{\text{RIS}}(\xi) d\xi, \quad \text{where } E^{\text{RIS}}(t) = \sum_{j=1}^N \frac{\|\mathbf{x}_{1,j}(t) - \mathbf{x}_{-1,j}(t)\|}{N}. \quad (24)$$

Here, T is a sufficiently large positive real number, t_r determines the transient of the numerical solution and $E^{\text{RIS}}(t)$ is the instantaneous synchronisation error. Since, we are interested to the correlation of the replica nodes between first (layer-(-1)) and third (layer-1) layers, the synchronisation error is calculated between the first and third identical pair of layers. To measure E^{RIS} , the time interval is taken over 1×10^5 units after an initial transient of 2×10^5 units, i.e., $t_r = 2000$ and $T = 1000$. In simulations, we have used the threshold value of E^{RIS} as 10^{-5} for synchrony.

The network (5) is numerically solved for $L = 1$ by using the Runge–Kutta–Fehlberg algorithm with integration time-step = 0.01. The codes are freely available for the readers to reproduce the numerical results [53]. The random structure of the layers is constructed by the probability $p = 0.1$ and initial conditions are chosen randomly from the phase-space. The effects of intralayer and interlayer coupling strengths, mismatch parameter in the local dynamics of the relay layer on the RIS are investigated. To draw all the numerical figures, we have taken 20 network realisations at each point, that is, the shown values of E^{RIS} are the average values with 20 network realisations. Also we identify the parameter regions for this RIS state, assessed by examining local asymptotic stability of each replica node among the layers- (± 1) .

The connectivity of the intralayer networks deliberate as the ER random network with the edge joining probability p and described by the Laplacian matrix $\mathcal{L}^{[l]}$. So each edge in the intralayer networks will be included with probability p and independent from the other edges. We have taken the intralayer inner coupling matrix for all the layers as the linear diffusive coupling through the first component of the state variable. Therefore, the element in the first row and first column of the intralayer inner-coupling matrix G is one and all

its other elements are zero. In other words, in the prescribed dynamical multiplex network (5), $G[\mathbf{x}_{l,j} - \mathbf{x}_{l,i}] = [x_{l,j} - x_{l,i} \ 0 \ 0]^T$, where $\mathbf{x}_{l,i} = [x_{l,i} \ y_{l,i} \ z_{l,i}]$ is a three dimensional state vector. The interlayer coupling is assumed to be diffusive through all the state variables. So, the interlayer inner-coupling matrix H is an identity matrix of order three and hence $H[\mathbf{x}_{k,i} - \mathbf{x}_{l,i}] = [x_{k,i} - x_{l,i} \ y_{k,i} - y_{l,i} \ z_{k,i} - z_{l,i}]^T$.

In the following parts, we explore the effect of the parameter mismatch in the local dynamics of the nodes and two different coupling strengths ϵ and η , on the emergence of the RIS state. We also explore the influence of the network parameter, namely p (ER network probability) on the RIS state. Now, we start our investigations with the numerical results and simultaneously we validate our obtained analytical findings. In the next two sub-sections, we choose two different paradigmatic chaotic oscillators one by one as the local dynamics of the nodes for numerical simulations.

5.1. Lorenz system

To numerically verify the role of impurity in the form of parameter mismatch in the middle layer for the emergence of RIS, we first consider three-layer multiplex network with local dynamic as Lorenz oscillators in each layer. So, mathematically the autonomous evolution equation of each isolate node is written as,

$$\begin{aligned}\dot{x} &= \sigma(y - x), \\ \dot{y} &= x(\rho - z) - y, \\ \dot{z} &= xy - \beta z.\end{aligned}\tag{25}$$

The system parameters are taken as $\sigma = 10$, $\beta = \frac{8}{3}$ and $\rho = 28$, for which each identical system is in a chaotic state. Here, the parameter ρ is chosen to have a mismatch in the middle layer, where $\Delta\rho$ is the amount of mismatch.

5.1.1. Relay interlayer synchronisation. In this case, we can write the transverse error dynamics of the RIS state as,

$$\begin{aligned}\delta\dot{x}_i &= \sigma(\delta y_i - \delta x_i) - \epsilon \sum_{j=1}^N \mathcal{L}_{ij}^{[1]} \delta x_j - \eta \delta x_i, \\ \delta\dot{y}_i &= \delta x_i(\rho - z_i) - x_i \delta z_i - \delta y_i - \eta \delta y_i, \\ \delta\dot{z}_i &= x_i \delta y_i + y_i \delta x_i - \beta \delta z_i - \eta \delta z_i,\end{aligned}\tag{26}$$

where $(\delta x_i, \delta y_i, \delta z_i) = (x_{1,i} - x_{-1,i}, y_{1,i} - y_{-1,i}, z_{1,i} - z_{-1,i})$ is the state variable of the i th node in the error system, and (x_i, y_i, z_i) is the state variable of the RIS manifold, whose equation of motion is

$$\begin{aligned}\dot{x}_i &= \sigma(y_i - x_i) - \epsilon \sum_{j=1}^N \mathcal{L}_{ij}^{[1]} x_j + \eta(x_{0,i} - x_i), \\ \dot{y}_i &= x_i(\rho - z_i) - y_i + \eta(y_{0,i} - y_i), \\ \dot{z}_i &= x_i y_i - \beta z_i + \eta(z_{0,i} - z_i).\end{aligned}\tag{27}$$

Also, the state variable $(x_{0,i}, y_{0,i}, z_{0,i})$ of the i th node in layer-0 satisfies the evolution equation

$$\begin{aligned}\dot{x}_{0,i} &= \sigma(y_{0,i} - x_{0,i}) - \epsilon \sum_{j=1}^N \mathcal{L}_{ij}^{[0]} x_{0,j} + 2\eta(x_i - x_{0,i}), \\ \dot{y}_{0,i} &= x_{0,i}(\rho + \Delta\rho - z_{0,i}) - y_{0,i} + 2\eta(y_i - y_{0,i}), \\ \dot{z}_{0,i} &= x_{0,i}y_{0,i} - \beta z_{0,i} + 2\eta(z_i - z_{0,i}).\end{aligned}\quad (28)$$

With the nonlinear equations (27) and (28), the linearised equation (26) is to be solved to compute all Lyapunov exponents. The maximum among these Lyapunov exponents (Λ_{\max}) as a function of ϵ , η and $\Delta\rho$ gives the necessary condition for the stability of the synchronous state. By adjusting these parameters for which $\Lambda_{\max} < 0$ gives stable RIS state. In the present instance, all the oscillators corresponding to each node of each layer remain chaotic before and after the critical values of the intralayer and interlayer coupling strengths.

Figure 2(a) shows the time evolution of the instantaneous synchronisation error $E^{\text{RIS}}(t)$ between the outer layers. Initially the parameter mismatch is set as zero, i.e., all the layers are now identical. In this situation, $E^{\text{RIS}}(t)$ never becomes zero. At time $t = 100$, the parameter mismatch $\Delta\rho$ is set as 2, and immediately $E^{\text{RIS}}(t)$ asymptotically converges to zero as time grows up. This clearly indicates the enhancement of the interlayer synchrony among the outermost layers due to the parameter mismatch in the relay layer. In this situation, we plot the phase-space in the $(x_{1,1}, x_{0,1})$ plane in figure 2(b), which clearly indicates that each node in the outer layer-1 is not synchronised with the counterpart node in the relay layer-0. However, each node in the layer-1 is synchronised with the counterpart node in the layer-(-1), verified by the plot of the projection of the synchronisation manifold in figure 2(c) in the $(x_{1,1}, x_{-1,1})$ plane.

In figure 2(d), we plot the time evolution of the state-variables $x_{0,1}(t)$ and $x_{1,1}(t)$, to investigate their dependency structure. Interestingly, we observe that they are in lag synchronisation with a tiny amplitude shift, i.e., phase-lag synchronisation. Therefore, each replica node in these two layers (outer and relay layers) has some kind of correlation among themselves. To characterise this correlation, we need to recall the following similarity function $S_{0,1}$ [54], as a time average of the difference between the variables $\mathbf{x}_{0,1}$ and $\mathbf{x}_{1,1}$, with the time-shift τ as,

$$S_{0,1}(\tau) = \sqrt{\frac{\langle [\mathbf{x}_{0,1}(t + \tau) - \mathbf{x}_{1,1}(t)]^2 \rangle}{\sqrt{[\langle \mathbf{x}_{0,1}^2(t) \rangle \langle \mathbf{x}_{1,1}^2(t) \rangle]}}}.\quad (29)$$

Numerically, we obtain the values of this function with respect to τ (figure 2(e)). Its global minimum $\sigma = \min_{\tau} \{S_{0,1}(\tau)\}$ for $\tau = \tau_0$ gives the amount of the lag among the two corresponding replica nodes. Here, $S_{0,1}(\tau)$ has a minimum for the non-zero time shift $\tau \simeq 0.006$, verifying a time-lag between these two replica nodes. It indicates a characteristics time shift $\tau = 0.006$ between $\mathbf{x}_{0,1}(t)$ and $\mathbf{x}_{1,1}(t)$ together with a tiny amplitude shift. As their amplitudes are uncorrelated, so the value of $S_{0,1}(\tau = 0.006)$ is relatively high (approximately 0.134). This regime of synchronisation is clear from figure 2(d). Therefore, the relay layer exhibits interlayer phase-lag synchronisation with the two outer layers, and the outer layers are in complete interlayer synchronisation state.

Now, we are interested to see the RIS region by changing the intralayer and interlayer coupling strengths ϵ and η together with the variation of parameter mismatch $\Delta\rho$. For this, we obtain the synchronisation region in the $(\epsilon, \Delta\rho)$ parameter space in figure 3 by taking four different interlayer coupling strengths. In figure 3(a), at $\eta = 2.1$, we observe that when $\Delta\rho = 0.0$,

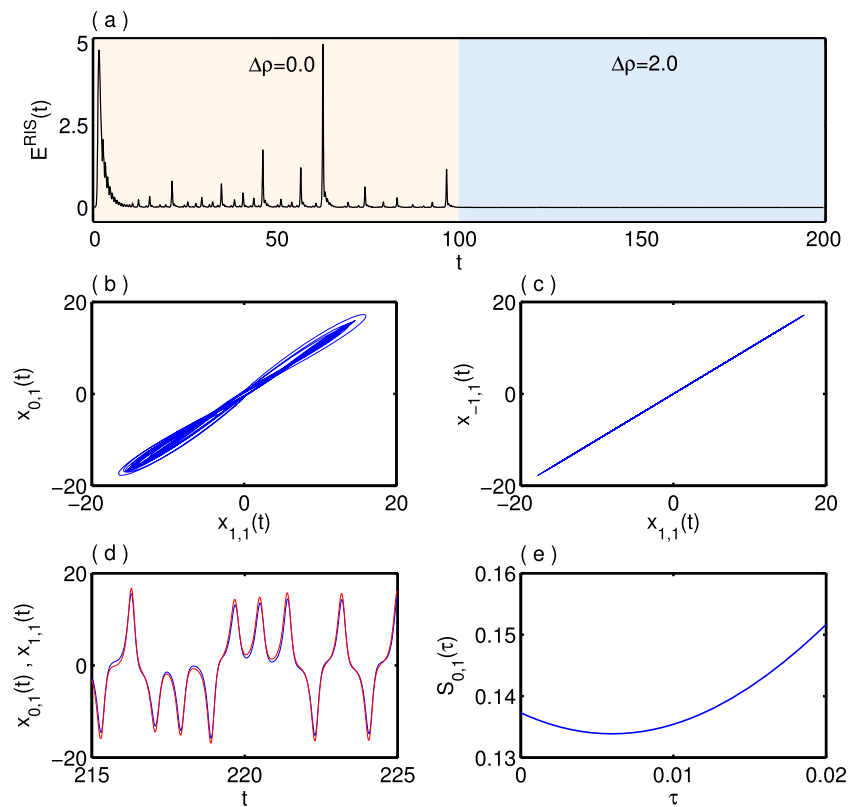


Figure 2. (a) Time evolution of the RIS error for $\Delta\rho = 0$ for time $t \in [0, 100]$ and $\Delta\rho = 2$ for time $t \in [100, 200]$. Projection of phase-space in the (b) $(x_{1,1}, x_{0,1})$ plane and (c) $(x_{1,1}, x_{-1,1})$ plane for $\Delta\rho = 2$. (d) Time evolution of the 1st node in the layer-0 and layer-1 depicting a phase-lag synchronisation and corresponding lag-similarity function $S_{0,1}(\tau)$ is plotted in (e) as a function of time-lag τ . Other parameter values are $p = 0.1$, $\epsilon = 0.1$ and $\eta = 2.5$. For the chosen coupling strengths, RIS between outer layers is not observed when three layers are identical. In presence of parameter mismatch ($\Delta\rho = 2$), the RIS emerges.

the critical value of ϵ for the emergence of relay interlayer synchrony is 0.174 and this synchronisation persists beyond the higher values of ϵ . However, by increasing the parameter mismatch $\Delta\rho$ from zero, the critical strength for ϵ gradually decreases. Finally, for $\Delta\rho = 4.5$, the relay interlayer synchrony arises for $\epsilon = 0.0$. The $(\epsilon, \Delta\rho)$ parameter region for higher value of $\eta = 2.3$ is delineated in figure 3(b). Here in the absence of the parameter mismatch, synchrony occurs at $\epsilon = 0.135$. Also like the previous sub-figure by increasing the parameter mismatch, the critical value of intralayer coupling strength gradually decreases. Finally at $\Delta\rho \geq 3.18$, the RIS can emerge in the absence of intralayer couplings. A similar type of result can be seen if we increase the interlayer coupling strength $\eta = 2.5$ in figure 3(c) and the synchronisation emerges when $\epsilon \geq 0.111$ for $\Delta\rho = 0.0$. However, when $\Delta\rho = 1.9$, the synchronisation between each replica node of the first and third layers emerges for $\epsilon = 0.0$. Also as we increase $\eta = 2.7$ in figure 3(d), the synchronisation region gradually increases. Therefore, the higher parameter mismatches give rise to larger synchronisation regions and enhancement of RIS state. Here the interesting finding is that the RIS region enlarges for a sufficient large intralayer coupling

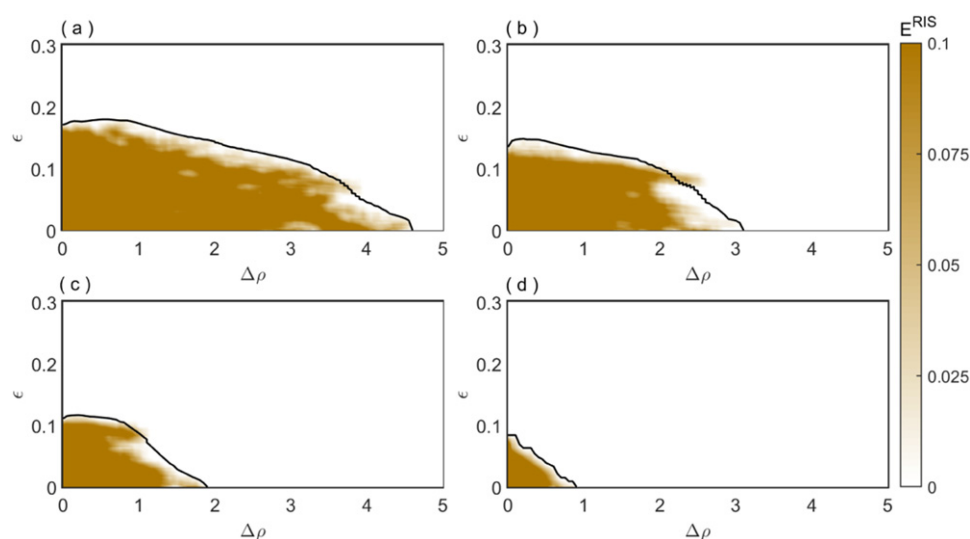


Figure 3. Effect of intralayer coupling strength ϵ and parameter mismatch $\Delta\rho$ on the transition of RIS and are characterised through the synchronisation error E^{RIS} for (a) $\eta = 2.1$, (b) $\eta = 2.3$, (c) $\eta = 2.5$, and (d) $\eta = 2.7$. The other parameter is fixed at $p = 0.1$. White and yellow regions respectively represent the stable and unstable RIS states. The MLE Λ_{\max} of the variational equation (6) gives the critical boundary for the RIS state. The black curve denotes the critical point for $\Lambda_{\max} = 0$. The above and below this curve represents the stable ($\Lambda_{\max} < 0$) and unstable ($\Lambda_{\max} > 0$) regions for the RIS state.

strength. It is physically reasonable that when nodes are strongly interacting within the layer compared to their replica layers, then it is obvious to relay their interlayer rhythmic adjustment which are reflected in this picture. Also, it gives the clue how to control the relay interlayer synchrony without effecting the interlayer connection. Remarkably, it is observed that the synchrony region in the $(\epsilon, \Delta\rho)$ plane enlarges for larger values of interlayer coupling strength between the layers.

Now, we verify the numerically obtained relay interlayer synchrony region (yellow regions in figure 3) in the $(\epsilon, \Delta\rho)$ parameter plane by the analytically obtained variational equation transverse to the RIS manifold (theorem 6). For this, the maximum transverse Lyapunov exponent Λ_{\max} is calculated from equation (26) along with equations (27) and (28). The critical curves of the RIS state characterised by $\Lambda_{\max} = 0$ are drawn by black lines in figures 3(a)–(d). In this parameter space, the above and below these curves respectively depict $\Lambda_{\max} < 0$ and $\Lambda_{\max} > 0$. Value of $\Lambda_{\max} < 0$ signifies the stable RIS state in the white region and $\Lambda_{\max} > 0$ gives the unstable synchrony state by the yellow region. These MLE plots are well agreed with the obtained numerical results. For all these cases, $\Lambda_{\max} = 0$ crosses the zero line approximately at those points where the RIS errors become zero, which indicates that our analytical local stability condition agrees well with our numerical simulations of the synchronisation error plots. However, there might be slight differences in the critical values for a close inspection due to the specific choice of the underlying intralayer network architectures. The whole stability analysis depends on the particular intralayer coupling structure and thus the boundaries also depends on this choice. This is why also the black lines depend on the particular realisation of the intralayer structure. More precisely for this stability analysis, the intralayer network

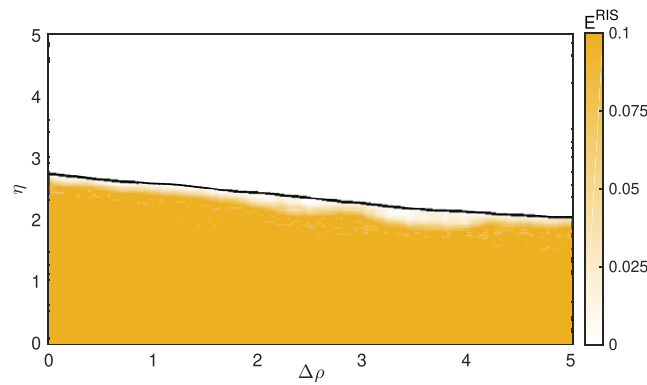


Figure 4. Two-dimensional phase diagram of the multiplex network with Lorenz oscillators in the $(\Delta\rho, \eta)$ parameter plane for the intralayer coupling strength $\epsilon = 0.1$. The RIS states are characterised by the synchronisation error E^{RIS} . Other parameter is fixed at $p = 0.1$. The black curve denotes the critical curve for $\Lambda_{\text{max}} = 0$. Below and above this curve respectively depict the unstable ($\Lambda_{\text{max}} > 0$) and stable ($\Lambda_{\text{max}} < 0$) regions for the RIS state.

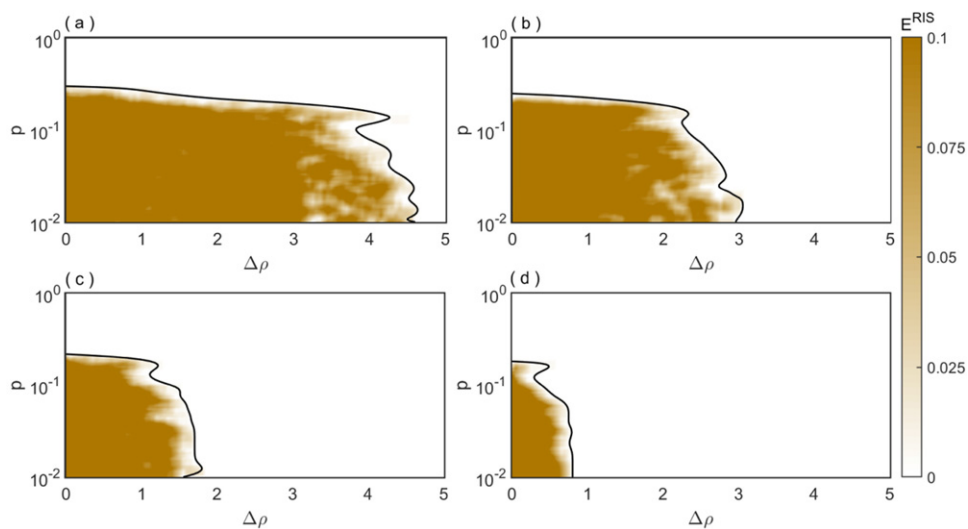


Figure 5. Variation of the RIS error E^{RIS} (color bar) in the $(\Delta\rho, p)$ parameter plane for the intralayer coupling strength $\epsilon = 0.05$ and the interlayer coupling strength: (a) $\eta = 2.1$, (b) $\eta = 2.3$, (c) $\eta = 2.5$, and (d) $\eta = 2.7$. Color bar represents the variation of E^{RIS} . The black lines are drawn at $\Lambda_{\text{max}} = 0$, which separate the regions of stable and unstable regions of RIS state. It is noted here that the region of synchronisation increases for higher value of interlayer coupling strength η .

architecture has been used with the same network parameter values (i.e., $N = 200$, and $p = 0.1$) to draw these black lines (similarly for other figures) which illustrate the analytical results.

Next, we investigate the emergence of relay interlayer synchrony under the simultaneous influences of interlayer coupling strength η and parameter mismatch $\Delta\rho$ in the relay layer. Figure 4 depicts the variation of interlayer synchronisation error in the $(\Delta\rho, \eta)$ parameter plane

for the intralayer coupling strength $\epsilon = 0.1$. From this figure, it is observed that by adding the inhomogeneity $\Delta\rho$ in the relay layer, the critical coupling strength for RIS reduces. To verify the obtained numerical parameter space, we calculate the MLE Λ_{\max} from the variational equation (26) with respect to $\Delta\rho$ and η . The critical curve of relay interlayer synchrony for which $\Lambda_{\max} = 0$ is shown by black line in figure 4. This critical curve is well-agreed with the numerically obtained error plot. The negative slope of the boundary in the $(\Delta\rho, \eta)$ plane confirms the enhancing effect of the RIS state.

Now we explore the influence of ER network probability p on the RIS state. Figure 5 shows the variations of the synchronisation error E^{RIS} by simultaneously varying the parameter mismatch $\Delta\rho$ and ER network probability p , for different values of interlayer coupling strength with fixed intralayer coupling strength $\epsilon = 0.05$. The value of p near to zero represents all the nodes of each layer are isolated, whereas it closer to one represents almost global network, and it denotes the ER topology for intermediate values of p in $(0, 1)$. At $\eta = 2.1$, figure 5(a) shows that when the oscillators in the outer layers are identical, then their corresponding replica nodes are completely synchronised at $p = 0.2884$. If we apply a small parameter mismatch $\Delta\rho$ in the middle layer, the synchronisation occurs for small values of p . At $\Delta\rho = 4.5$, each replica of the first and third layers are synchronised for $p = 0.01$. We have also examined this trend for $\eta = 2.3$, $\eta = 2.5$, and $\eta = 2.7$ at which the network has larger interlayer synchronisation region and the results are shown in figures 5(b)–(d), respectively. The stability region of the relay interlayer synchrony is also verified by plotting $\Lambda_{\max} = 0$ black curve in the parameter space $(\Delta\rho, p)$ for $\eta = 2.1$, $\eta = 2.3$, $\eta = 2.5$, and $\eta = 2.7$ in figures 5(a)–(d), respectively. The region above the black curve is the stable region of the RIS state. This critical curve is an excellent agreement with the numerical simulation.

For the global stability of the RIS state, we consider interlayer inner-coupling matrix as the identity matrix, and hence minimum eigenvalue of the matrix H is $\lambda_{\min}(H) = 1$. For the chosen system parameter values of the two outer layers, the Lipschitz constant of the Lorenz oscillator is approximately 22.3. Therefore, in this case the required global stability condition reduces as $\eta > 22.3$. For $\eta > 3$, this state emerges for initial conditions that are infinitesimally close to the associated synchronisation manifold \mathcal{S}^{RIS} in figure 4. However, the derived global stability condition (theorem 13) ensures that \mathcal{S}^{RIS} is stable with respect to any arbitrary perturbation from its transverse sub-space if $\eta > 22.3$. For $\eta < 3$, the RIS is an unstable solution, however, the initial condition is close to \mathcal{S}^{RIS} . When $\eta \in (3, 22.3)$, it becomes stable only for infinitesimal perturbation of the initial condition, but may be multi-stable for any random perturbations. Such multi-stability can be measured using the basin stability framework, which is beyond the focus of this work. For our chosen coupling functions and network consisting of Lorenz oscillators, the stability can be assured for any random perturbations when $\eta > 22.3$.

This Lyapunov-based method provides a sufficient condition for global stability. Therefore, the critical coupling strength obtained from this approach is usually far away from the exact critical coupling strength required for global stability. However, one may construct more suitable Lyapunov functions to optimise the global stability condition. For such purpose, the Lyapunov optimisation technique could be an appropriate tool, which refers to use the Lyapunov function optimally in order to control a dynamical system.

5.1.2. Demultiplexing effect. Now, we numerically explore the effect of demultiplexing on the RIS state. To verify our analytical results (lemma 14 and theorem 15) on the demultiplexing of interlayer connections, we systematically demultiplex the interlayer connections one-by-one until the three layers become isolated. To numerically verify the lemma 14, we first demultiplex a particular node (say, 1st node), i.e., we remove the interlayer connections of the 1st node between three layers.

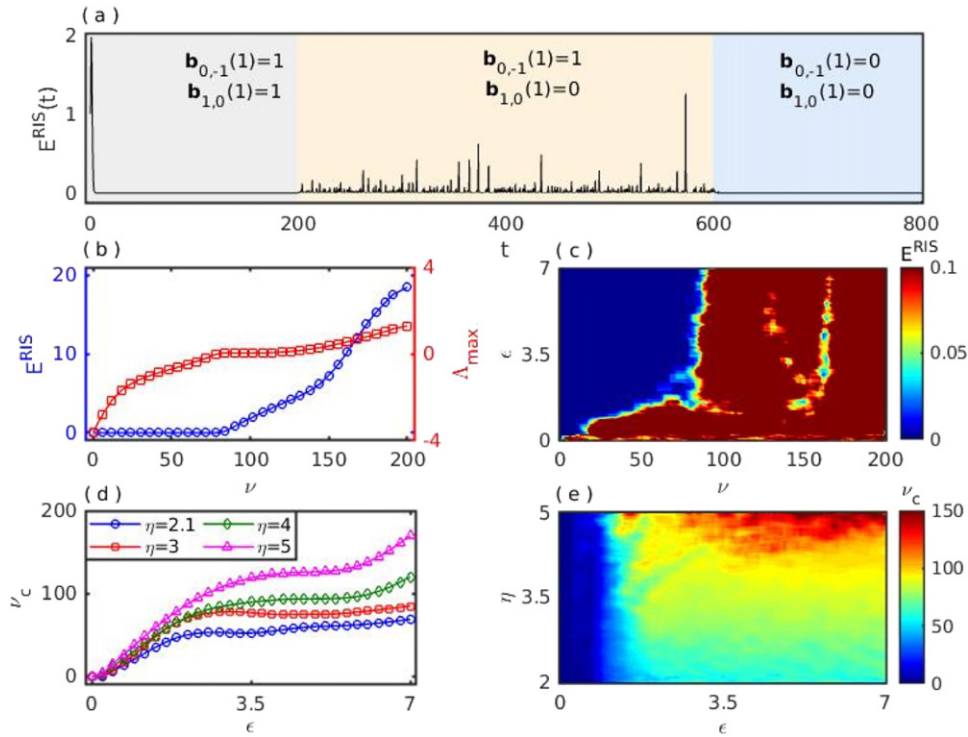


Figure 6. (a) Time evolution of the RIS error $E^{\text{RIS}}(t)$ by demultiplexing interlayer connections among the three layers : during the time-interval $t \in [0, 200]$, $\mathbf{b}_{1,0}(1) = 1$, $\mathbf{b}_{0,-1}(1) = 1$; $t \in [200, 600]$, $\mathbf{b}_{1,0}(1) = 1$, $\mathbf{b}_{0,-1}(1) = 0$ and $t \in [600, 800]$, $\mathbf{b}_{1,0}(1) = 0$, $\mathbf{b}_{0,-1}(1) = 0$; with $\epsilon = 2.0$, $\eta = 3.0$ and $\Delta\rho = 3.0$. (b) Variation of E^{RIS} (left axis, blue circle curve) and Λ_{max} (right axis, red square curve) with respect to the number of demultiplex replicas ν for $\epsilon = 3.5$. (c) RIS region in the (ϵ, ν) parameter space, where the color bar denotes the variation of E^{RIS} . For the middle panel sub-figures (b) and (c), other parameters are fixed at $p = 0.1$, $\eta = 3.0$ and $\Delta\rho = 3.0$. (d) Critical number of demultiplex replicas ν_c as a function of ϵ for $\eta = 2.1$, $\Delta\rho = 2.1$ (blue circle curve), $\eta = 3.0$, $\Delta\rho = 3.0$ (red square curve), $\eta = 4.0$, $\Delta\rho = 4.0$ (green diamond curve) and $\eta = 5.0$, $\Delta\rho = 5.0$ (magenta triangle curve). (e) Critical number of demultiplex replicas in the (ϵ, η) parameter space where the color bar represents the variation of ν_c . For the bottom panel sub-figures (d) and (e), $\Delta\rho = \eta$ and $p = 0.1$.

The time-evaluation of the instantaneous RIS error $E^{\text{RIS}}(t)$ of the demultiplexed network is drawn in figure 6(a). During the time-interval $t \in [0, 200]$, all the interlayer connections are present, i.e., the network is fully multiplex. For such structure at fixed $\epsilon = 2.0$, $\eta = 3.0$ and $\Delta\rho = 3.0$, all the replica nodes between the layer-1 and layer-(-1) asymptotically converges to each other. At time $t = 200$, the replica connection of the 1st node in layer-0 with its counterpart node in layer-(-1) is removed, but the interlayer connection of the 1st node between layer-0 and layer-(-1) is present. In this structure, $\mathbf{b}_{1,0}(1) = 1$ and $\mathbf{b}_{0,-1}(1) = 0$, however $\mathbf{b}_{1,0}(i) = \mathbf{b}_{0,-1}(i) = 1$ for $i = 2, 3, \dots, N$. Due to broken of symmetry in the interlayer connection of the 1st node between three layers, the synchronisation error $E^{\text{RIS}}(t)$ becomes non-zero and RIS state becomes unstable. This confirms our analytically derived invariance condition in lemma 14. Again at $t = 600$, the replica connection of the 1st node in the layer-(-1) with its counterpart node in the layer-0 is removed. For such case, $\mathbf{b}_{1,0}(1) = \mathbf{b}_{0,-1}(1) = 0$

and $\mathbf{b}_{1,0}(i) = \mathbf{b}_{0,-1}(i) = 1$ for $i = 2, 3, \dots, N$; then the multiplex network becomes symmetry again and the solution asymptotically converges to the synchronisation manifold S^{RIS} . The above fact indicates that under appropriate demultiplexing of the replica node, the RIS is robust. This state will be an invariant solution under progressive demultiplexing if we remove each pair of replica in the triplex network. However, by removing any one of the pair, this state will not be an invariant solution. This numerical illustration verifies lemma 14 for triplex network.

Here, demultiplexing is done by removing the two interlayer links of a particular node simultaneously between three layers. In left axis of figure 6(b), we plot the variation of E^{RIS} by successively demultiplexing the replica connections until all the three layers become uncoupled for $\epsilon = 3.5$. Here, ν represents the number of demultiplex replicas and $0 \leq \nu \leq N$. Here, we can demultiplex at most 78 replicas in order to maintain the RIS state. Right axis of figure 6(b) represents the variation of the associated maximum transverse Lyapunov exponent Λ_{max} with respect to ν . Λ_{max} remains negative up to $\nu = 78$. Beyond that value of ν , Λ_{max} crosses the zero line, and becomes positive. Thus the analytically derived local stability condition in theorem 15 for demultiplex replicas is well agreed with the numerical simulations.

We have also checked that, for $\epsilon = 0.5$, we can demultiplex at most 20 replicas to preserve this synchronisation pattern. Moreover, for $\epsilon = 2.0$, we can demultiplex 54 replica connections at most, and still maintain RIS. Therefore, by increasing ϵ , the number of demultiplex replicas gradually increases. To investigate more about this monotonic tendency, we plot the variation of E^{RIS} in the (ϵ, ν) parameter space for $\eta = 3.0$ and $\Delta\rho = 3.0$ in figure 6(c). Here, up to $\epsilon = 3.25$, the critical number of demultiplex replicas rapidly increases by gradually increasing ϵ from zero. Beyond that it increases quite gradually up to $\epsilon = 7.0$. This figure explicitly demonstrates that the critical value of ν up to which relay interlayer synchrony is stable and improves considerably as ϵ increases. By increasing the intralayer coupling strength ϵ , the number of interlayer links that may be removed increases while relay interlayer synchrony is still preserved.

Now we find the critical value ν_c of the demultiplex interlayer link below which the synchronisation manifold S^{RIS} is stable. In figure 6(d), we plot the critical number of demultiplex replicas ν_c for which the RIS state persists, with respect to ϵ for different values of η and $\Delta\rho$. At $\eta = 2.1$ and $\Delta\rho = 2.1$, as ϵ increases ν_c also gradually increases (blue circle curve) from zero at $\epsilon = 0$. Finally, at $\epsilon = 7.0$, we can demultiplex at most 69 replicas. The red square curve is plotted for $\eta = 3.0$ and $\Delta\rho = 3.0$, here also ν_c gradually increases and at $\epsilon = 7.0$, we can demultiplex maximum 85 replica connections. For $\eta = 4.0$ and $\Delta\rho = 4.0$, the variation of ν_c is plotted by the green diamond curve. In this case, as ϵ gradually increases, ν_c also monotonically increases, and at $\epsilon = 7.0$, ν_c becomes 120. By taking $\eta = 5.0$ and $\Delta\rho = 5.0$, the same increasing tendency of ν_c is observed with respect to ϵ . Here, we can able to demultiplex 170 replica connections for $\epsilon = 7.0$. Therefore, ν_c monotonically increases with respect to both ϵ and η . For better visualisation of this demultiplex scenario, we plot ν_c in the (ϵ, η) parameter space in figure 6(e), where the color bar represents the variation of ν_c . The monotonic increasing tendency of ν_c by gradually raising either ϵ or η has depicted more clearly from the figure 6(e). From the above analysis, it is clear that $(N - \nu_c)$ number of interlayer links are sufficient to maintain RIS state between the outer layers.

5.2. Rössler system

To further elucidate the heterogeneous middle layer plays a key role for enhancing the critical interlayer coupling strength for the emergence of RIS, we consider a three-layer multiplex network with each node is associated with the Rössler oscillators as local dynamics. The equation

of the local dynamics is

$$\begin{aligned}\dot{x} &= -\omega y - z, \\ \dot{y} &= \omega x + \alpha y, \\ \dot{z} &= \beta + z(x - c).\end{aligned}\tag{30}$$

Here, the parameter values are fixed at $\alpha = 0.2$, $\beta = 0.4$, $c = 7.5$ and $\omega = 1$ for which the isolate system is in chaotic state. The parameter ω is chosen as the mismatch parameter such that it has the value of $\omega + \Delta\omega$ in the middle layer, i.e., $\Delta\omega$ represents the parameter mismatch in the middle layer. A fixed initial conditions for each node is chosen randomly from the subspace $[-0.01, 0.01] \times [-0.01, 0.01] \times [0, 0.01]$ where all the oscillators are considered as in small perturbations for the local stability of the RIS.

In coupled Rössler oscillators with the identity inner-coupling matrix, if synchronisation once occurs then it persists for higher coupling strengths [55]. As we consider the inter-layer inner-coupling matrix as identity matrix, therefore, in the absence of intralayer coupling ($\epsilon = 0$), Λ_{\max} has only one cross point along the η -axis, and it remains negative for further large- η limit. Interestingly, highly rich complex behavior arises when $\eta \neq 0$, we consider the intralayer connections and non-identical parameter value in the middle layer. Now, we investigate the effect of different parameters on the relay interlayer synchrony state and demonstrate the results in figures 7 and 8.

We fixed the intralayer and interlayer coupling strengths at $\epsilon = 0.005$ and $\eta = 0.06$, for which the RIS not emerge. The time evolution of the instantaneous RIS error $E^{\text{RIS}}(t)$ is plotted in figure 7(a) by varying the parameter mismatch $\Delta\omega$. For the time $t \in [0, 1000)$, the parameter mismatch $\Delta\omega$ is set as 0, i.e., during this time all the three layers are identical. During this time interval, $E^{\text{RIS}}(t)$ remains non-zero. Hence, the RIS state does not observe at this time duration for the chosen coupling strengths and other parameters. At time $t = 1000$, the value of $\Delta\omega$ is set as 0.1. Now the middle layer has a parameter mismatch with the other two layers. Then $E^{\text{RIS}}(t)$ asymptotically converges to zero as time increases. Therefore, the parameter mismatch induces the RIS state. In figure 7(b), the projection of the phase space is plotted in the $(\mathbf{x}_{1,1}, \mathbf{x}_{0,1})$ plane to show no synchronisation between outer layers and middle relay layer. However, the projection of the phase-space in the $(\mathbf{x}_{1,1}, \mathbf{x}_{-1,1})$ plane shows synchronisation between them, the corresponding synchronisation manifold is shown in figure 7(c). Similarly, we have checked that this synchronisation preserves for all other replica nodes of the outer layers.

Interestingly, each replica node between the layer-1 and layer-0 is in lag synchronisation with an amplitude shift depicted in figure 7(d). To find the lag time numerically, we calculate the lag-similarity function with respect to τ in figure 7(e). Here, $S_{0,1}(\tau)$ has a global minimum for the non-zero time shift $\tau \simeq 0.54$ which signifies a time-lag between $x_{0,1}(t)$ and $x_{1,1}(t)$. As their amplitudes are uncorrelated, so the value of $S_{0,1}(\tau = 0.54)$ is relatively high. This regime of synchronisation is clearly demonstrated in figure 7(d). This indicates that a common parameter mismatch in each node of the relay layer creates phase-lag synchronisation among each replica nodes of the two outer layers leads to an enhancement of the synchronisation among each replica in the outer layers. Now we investigate the effect of the interlayer coupling strength η and parameter mismatch $\Delta\omega$ on the RIS.

In order to have a general view of the effect of the parameters variations on this synchronisation state, we have drawn two-dimensional phase diagram in the $(\Delta\omega, \eta)$ parameter plane for $\epsilon = 0.03$ in figure 8. In this diagram, variation of the error E^{RIS} is shown by the color bar where the white region indicates $E^{\text{RIS}} \simeq 0$ which refers to the replica-wise complete synchrony of layer-1 and layer-(-1). The RIS is obtained by increasing the interlayer coupling strength η . Interestingly, by applying a parameter mismatch $\Delta\omega$ in the local dynamics of the middle layer,

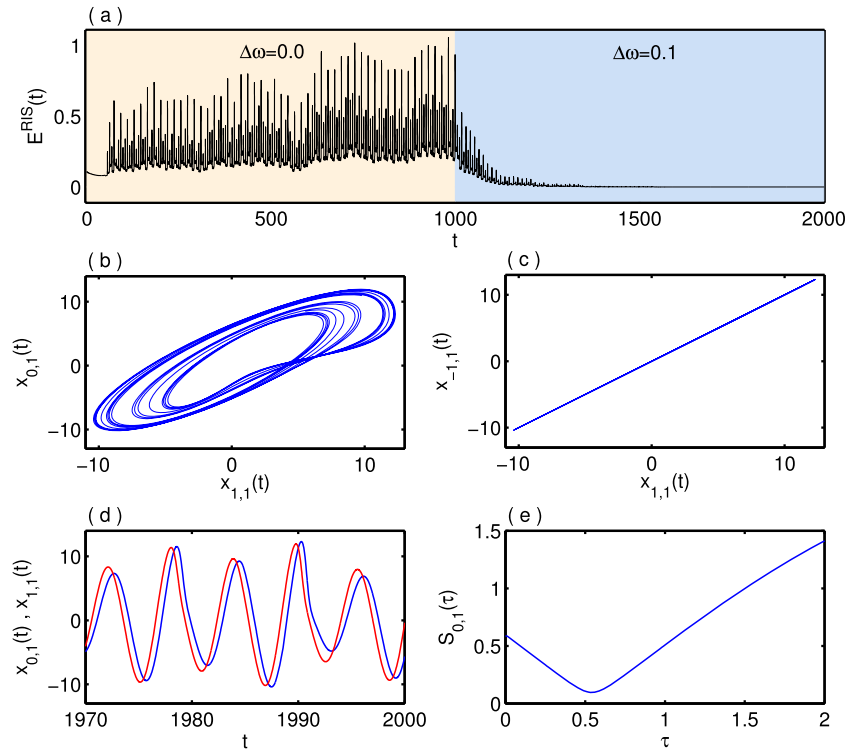


Figure 7. (a) Time evolution of the RIS error E^{RIS} for $\Delta\omega = 0.0$ at the time $t \in [0, 1000]$ and $\Delta\omega = 0.1$ for time $t \in [1000, 2000]$ for the Rössler network. Projection of the phase-space for $\Delta\omega = 0.1$ in the (b) $(x_{0,1}, x_{1,1})$ plane shows no correlation among the replica nodes of the outer layer and the relay layer, (c) the $(x_{1,1}, x_{-1,1})$ plane shows synchronisation among the two outer layers. (d) Time evolution of the 1st node of layer-0 and layer-1 depicting a lag synchronisation with an amplitude shift, the corresponding lag-similarity function $S_{0,1}(\tau)$ is plotted in (e) as a function of time-lag τ . The other parameter values: $p = 0.1$, $\epsilon = 0.005$ and $\eta = 0.06$.

the RIS threshold η is decreased. To verify the numerically obtain parameter region in figure 8, we calculate the MLE Λ_{\max} from the analytically calculated variational equation (6). Here, the critical curve for which $\Lambda_{\max} = 0$ is drawn by the black curve. Therefore, the regions below and above this curve denote unstable ($\Lambda_{\max} > 0$) and stable ($\Lambda_{\max} < 0$) regions, respectively.

As the interlayer inner-coupling matrix is the identity matrix, so the corresponding matrix H is the identity matrix and hence $\lambda_{\min}(H) = 1$. For the chosen system parameter of the two outer layers, the Lipschitz constant of the Rössler oscillator is approximately 26.53. Therefore, we can achieve a globally stable RIS state for $\eta > 26.53$. This condition is sufficient and much higher than the local stability condition.

6. Numerical results for five-layer (i.e., $L = 2$) multiplex network

Now, we numerically validate the analytical findings by means of a multiplex network consisting of five layers, i.e., $L = 2$. Here, the local dynamics of the nodes in the middlemost layer (layer-0) contains parameter mismatch and the local dynamics in the symmetric position

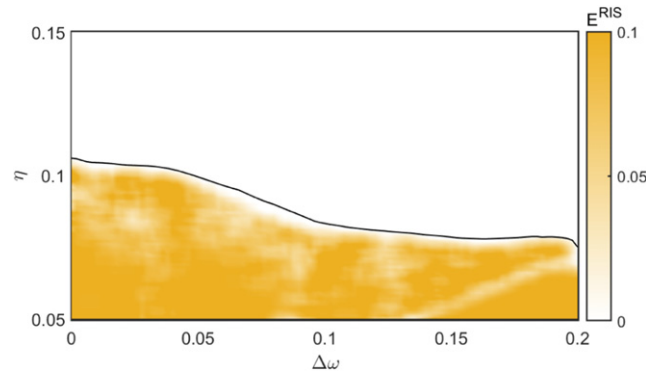


Figure 8. The two-dimensional phase diagram of the RIS state in $(\Delta\omega, \eta)$ parameter plane for $\epsilon = 0.03$. The color bar indicates the variation of E^{RIS} . The black curve is the critical curve for which $\Lambda_{\text{max}} = 0.0$; the regions below and above of this curve respectively denote the regions of unstable ($\Lambda_{\text{max}} > 0$) and stable ($\Lambda_{\text{max}} < 0$) synchronisation state. The probability of the ER network is set at $p = 0.1$.

layers are identical, but different from the middlemost layer. Similar to the three-layer case, we consider Lorenz oscillators as the local dynamics of each individual nodes. However, the intralayer network configurations (ER network), coupling function (through x -variable), and the interlayer coupling function are the same as for the three-layer cases. Here, an impurity in the form of parameter mismatch is introduced with amount $2\Delta\rho$ and $\Delta\rho$ respectively for middle-most layer (layer-0) and the immediate nearest layers (layer- (± 1)).

In the following parts, we study the RIS states between symmetric position layers (i.e., layer- ± 1 and layer- ± 2) by varying the coupling strengths ϵ, η and also parameter mismatch $\Delta\rho$.

6.1. Relay interlayer synchronisation

The time evolution of the instantaneous relay synchronisation error $E^{\text{RIS}}(t)$ is plotted in figure 9(a) by taking two different values of $\Delta\rho$. From $t = 0$ to $t = 1000$, all the five layers are identical, i.e., $\Delta\rho = 0$. In this course of time, $E^{\text{RIS}}(t)$ remains nonzero. When at time $t = 1000$, the values of $\Delta\rho$ is placed at 2.5, $E^{\text{RIS}}(t)$ becomes zero after very short transient. Therefore, the parameter mismatch among the replica nodes induces the RIS for this five-layer multiplex network. At this time, we plot the phase space in the $(x_{1,1}, x_{0,1})$ and $(x_{1,1}, x_{2,1})$ plane in figures 9(b) and (c), respectively. These two figures depict that each node in layer-1 is not synchronised neither with its replica nodes in the layer-0 and nor in layer-2. However, the projection of the phase space plot in the $(x_{1,1}, x_{-1,1})$ (in figure 9(d)) plane verifies that each node in the layer-1 is synchronised with the replica node in the layer- (-1) . Similarly, layer-2 and layer- (-2) are also in interlayer synchronisation state.

To investigate their dependency structure, we plot the time-evolution of the state-variables $x_{0,1}(t)$, $x_{1,1}(t)$ and $x_{2,1}(t)$ in figure 9(e). Here we observe that there are some kind of correlation among the replica nodes in these three layers. With a very small amplitude deviation, they are in lag synchronisation state. To characterise these lag synchronisations, we plot the respective lag-similarity functions in the lower panel of figure 9. The interlayer lag synchronisation among

layer- l and layer- m is characterised by the similarity function $S_{l,m}(\tau) = \sqrt{\frac{\langle [\mathbf{x}_{l,1}(t+\tau) - \mathbf{x}_{m,1}(t)]^2 \rangle}{\langle \mathbf{x}_{l,1}^2(t) \rangle \langle \mathbf{x}_{m,1}^2(t) \rangle}}$,

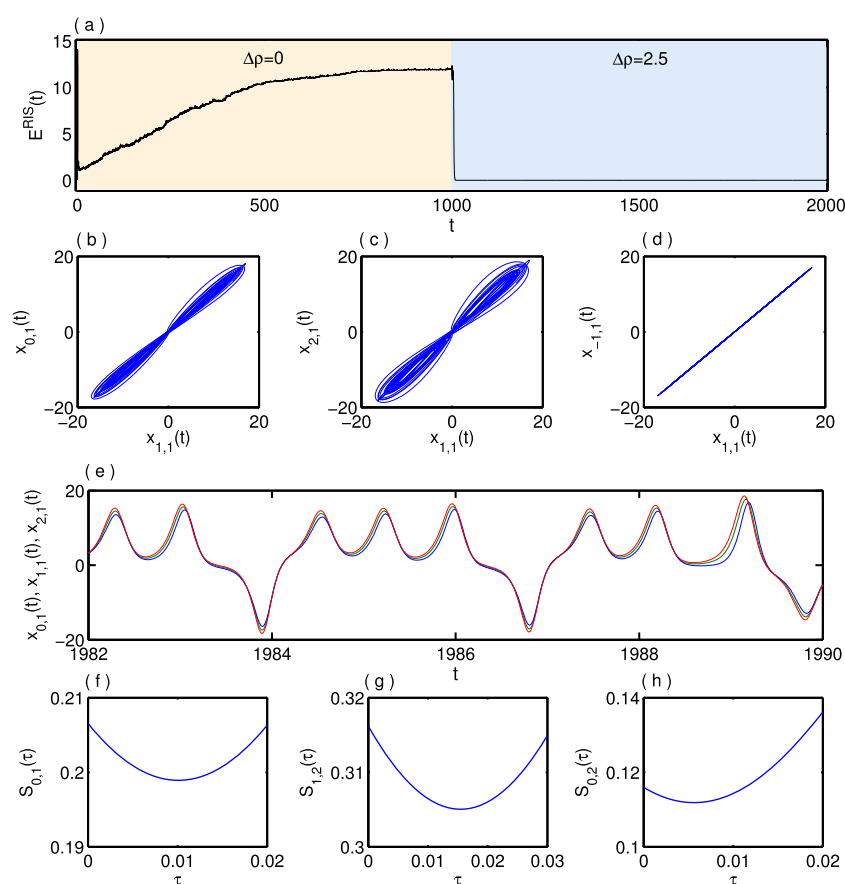


Figure 9. (a) Time evolution of the RIS error E^{RIS} for $\Delta\rho = 0$ at the time $t \in [0, 1000]$ and $\Delta\rho = 2.5$ for time $t \in [1000, 2000]$. Projection of the phase-space for $\Delta\rho = 2.5$ in the (b) $(x_{1,1}, x_{0,1})$ and (c) $(x_{1,1}, x_{2,1})$ planes show no synchronisation among the replica nodes in the layer-0, layer-1 and layer-2 while (d) the $(x_{1,1}, x_{-1,1})$ plane shows interlayer synchronisation among the layer- ± 1 . (e) Time evolutions of the 1st node of layer-0 (blue curve), layer-1 (red curve) and layer-2 (green curve) depicting a phase-lag synchronisation, the respective lag-similarity functions are plotted in (f)–(h) as a function of time-lag τ . The other parameter values: $p = 0.1$, $\epsilon = 0.01$ and $\eta = 3.27$.

for $l < m$ and $l, m \in \{0, 1, 2\}$. In figure 9(f), $S_{0,1}(\tau)$ has a minimum value for $\tau \simeq 0.01$, indicates that there is time-shift $\tau \simeq 0.01$ with a small amplitude deviation between the two state variables $\mathbf{x}_{0,1}(t)$ and $\mathbf{x}_{1,1}(t)$. Similarly, the lag similarity functions among layer-1, layer-2 and layer-0, layer-2 are plotted in figures 9(g) and (h). Now, $S_{1,2}(\tau)$ and $S_{0,2}(\tau)$ has respective minimum value at $\tau \simeq 0.0155$ and $\tau \simeq 0.005$. Therefore, the symmetric positions layers are in interlayer synchronisation states and the non-symmetric positions layers are in interlayer phase-lag synchronisation states.

Here, the interlayer synchronisations occur among the layer- (± 1) and the layer- (± 2) . The interlayer synchronisation errors of the two pairs of symmetric positions layers, layer- (± 1) and layer- (± 2) , are plotted with respect to η in figure 10(a) for $p = 0.1$. Here, $E_{\pm m}^{\text{inter}}$ denotes the interlayer synchronisation error of the pair of layer- $(\pm m)$, which is defined

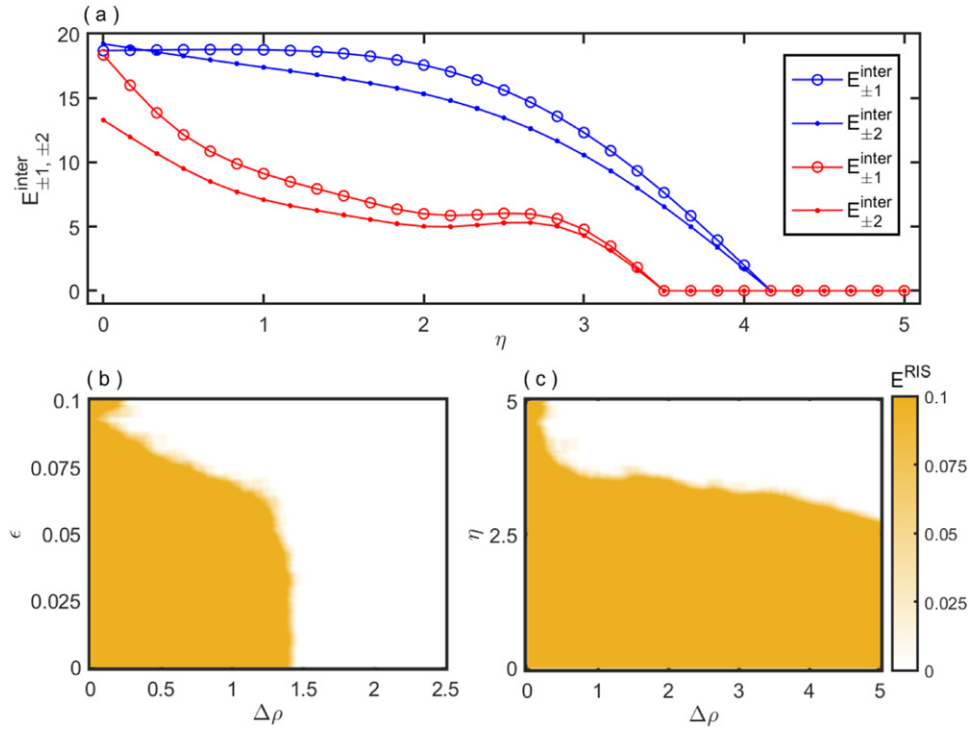


Figure 10. (a) Variation of $E_{\pm 1}^{inter}$ (hollow circle curves) and $E_{\pm 2}^{inter}$ (solid circle curves) with respect to η for $\Delta\rho = 1.5$, $\epsilon = 0.05$ (blue curves) and $\Delta\rho = 2.5$, $\epsilon = 0.1$ (red curves). These curves show that the RIS among symmetric positions layers occur at the same interlayer coupling strength η . (b) Variation of E_{RIS} in the parameter space of $(\Delta\rho, \epsilon)$ for $\eta = 5.0$. (c) RIS region in the $(\Delta\rho, \eta)$ parameter plane in terms of the corresponding synchronisation error E_{RIS} for $\epsilon = 0.1$. The probability of the ER networks for intralayer networks is fixed at $p = 0.1$.

as $E_{\pm m}^{inter} = \lim_{T \rightarrow \infty} \frac{1}{T} \int_0^T \sum_{j=1}^N \frac{\|\mathbf{x}_{m,j}(t) - \mathbf{x}_{-m,j}(t)\|}{N} dt$ for $m = 1, 2$. Here, blue curves depict the variation of $E_{\pm 1}^{inter}$ (hollow circle curve) and $E_{\pm 2}^{inter}$ (solid circle curve) for $\Delta\rho = 1.5$ and $\epsilon = 0.05$ with respect to η . $E_{\pm 1}^{inter}$ and $E_{\pm 2}^{inter}$ both touch the zero line at $\eta = 4.167$, i.e., same values of η . Similarly, red curves depict the variation of $E_{\pm 1}^{inter}$ (hollow circle curve) and $E_{\pm 2}^{inter}$ (solid circle curve) for $\Delta\rho = 2.5$ and $\epsilon = 0.1$ with respect to η . Also, we observe an enhancement of the interlayer synchronisation states among the symmetric position layers. Moreover, $E_{\pm 1}^{inter}$ and $E_{\pm 2}^{inter}$ become zero exactly at the identical value of η ($\eta = 3.5$). Therefore, as η gradually increases, the interlayer synchronisation of the two pairs of symmetric position layers occur simultaneously. This numerical result verifies the analytical result derived in lemma 4 for five layers for the simultaneous occurrence of interlayer synchronisation between the symmetric position layers.

In figure 10(b) we draw the parameter diagram of the RIS state in the $(\Delta\rho, \epsilon)$ parameter plane for $\eta = 5.0$. The color bar denotes the continuous variation of E_{RIS} . Here, increasing values of either ϵ or $\Delta\rho$ gradually enlarges the RIS region. This means that larger values of the intralayer coupling strength ϵ or the parameter mismatch $\Delta\rho$ decrease the critical synchrony threshold on the interlayer coupling strength η . Next, the simultaneous influence of parameter

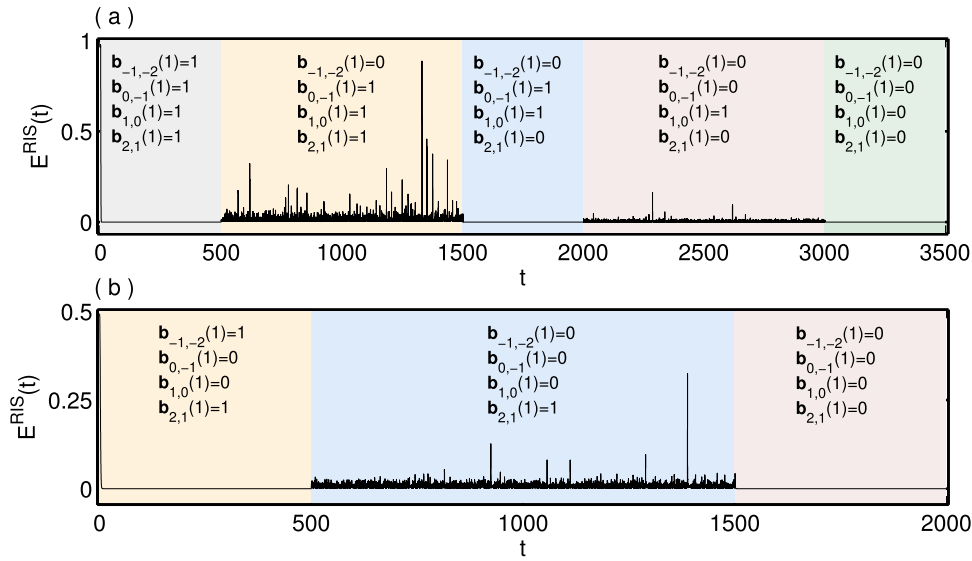


Figure 11. Time evolution of $E^{\text{RIS}}(t)$ by successively demultiplexing the interlayer connections among the five layers. (a) During the time-interval $t \in [0, 500)$, we keep all the replica connections in the pentaplex network. During $t \in [500, 1500)$, the replica connection among the first node of layer-(-2) and layer-(-1) is removed. Again during $t \in [1500, 2000)$, replica link among the first node of layer-1 and layer-2 has been withdrawn. During $t \in [2000, 3000)$, the first replica link among the layer-0 and layer-(-1) has been removed. Finally, during $t \in [3000, 3500]$, the first replica connection among the layer-0 and layer-1 has been removed. (b) During the time interval $t \in [0, 500)$, only the replica links among the first node of layer-0, layer-(-1), and layer-0, layer-1 has been removed, however, all other replica links are resent. Then during $t \in [500, 1500)$, we remove the first replica connection among the layer-(-1) and layer-(-2). Finally, during $t \in [1500, 2000)$ we removed the replica link among the first node of layer-1 and layer-2. All the parameter values are fixed at: $\epsilon = 2.0$, $\eta = 3.5$, $\Delta\rho = 2.5$ and $p = 0.1$.

mismatch $\Delta\rho$ and interlayer coupling strength η is presented in figure 10(c) in terms of the corresponding synchronisation error E^{RIS} for $\epsilon = 0.1$. As like triplex networks, the critical interlayer coupling threshold here also enlarges the emergence of the RIS state by introducing the parameter mismatches among the layers.

6.2. Demultiplexing effect

Now we study the robustness of the RIS state of the five-layer multiplex network with respect to the interlayer replica connections. To verify lemma 14, we demultiplex the interlayer connections of the first node in each layer in two different ways. We fix the parameter values at $\epsilon = 2.0$, $\eta = 3.5$, $\Delta\rho = 2.5$ and $p = 0.1$, for which RIS observe between symmetric position layers. The time-evaluations of $E^{\text{RIS}}(t)$ are drawn in figure 11 by demultiplexing the interlayer connections of the 1st replica node in the five layers by two different ways. In figure 11(a), we keep all the interlayer connections among the five layers during the time-interval $t \in [0, 500)$. For such structure, $\mathbf{b}_{l+1,l}(i) = 1$ for all $l = -2, -1, 0, 1$ and $i = 1, 2, \dots, 200$. Here, the interlayer synchronisation emerges among the two pairs of layers: layer-(-1) and layer-(-2) after a very small transient time. At time $t = 500$, the replica connection of the 1st node in the layer-(-2) with its counterpart node in layer-(-1) is only removed. For such structure, $\mathbf{b}_{-1,-2}(1) = 0$,

but $\mathbf{b}_{2,1}(1) = 1$. As soon as the removal of this replica connection, the solution of the entire multiplex network leaves the manifold \mathcal{S}^{RIS} and does not return further due to broken of symmetry in the interlayer connection. At the time $t = 1500$, the 1st replica connections among layer-2 and layer-1 is removed by setting $\mathbf{b}_{2,1}(1) = 0$ and again the solution regresses to \mathcal{S}^{RIS} . Now, at time $t = 2000$, the 1st replica connection among layer-0 and layer-(-1) is removed (i.e., $\mathbf{b}_{0,-1}(1) = 0$). Due to the loss of symmetry in the interlayer connections with respect to the middlemost layer, the solution once again leaves the manifold \mathcal{S}^{RIS} and becomes unstable. Then it returns to \mathcal{S}^{RIS} , when we remove the corresponding replica connection among layer-1 and layer-0 at time $t = 3000$. This numerical investigation confirms the analytically derived invariance conditions in lemma 14 for the RIS state due to progressive demultiplexing of replicas.

To further illustrate this fact, we again demultiplex the replica connections in a different way. During the time interval $t \in [0, 500)$, all the interlayer replica connections are present except the interlayer connections among the 1st nodes in layers 0, (-1) and the layers-1, 0. In this case, immediately the solution converges to \mathcal{S}^{RIS} . Albeit, the solution leaves \mathcal{S}^{RIS} when we remove the replica connection of the 1st node in layers (-1), (-2), while keeping the corresponding replica connection in the layers-2, 1. Finally, at $t = 1500$, when removing these replica links and the solution come-back to the manifold \mathcal{S}^{RIS} . Therefore, the RIS state can also emerge in the pentaplex configurations, provided the symmetry condition on the interlayer connections hold.

Next, we systematically demultiplex the interlayer connections until the five layers become disconnected. The demultiplexing procedure can be done in three different ways:

- Removing the interlayer connections of the two layers ± 1 with their subsequent layer, i.e., by simultaneously setting $\mathbf{b}_{0,-1}(i) = \mathbf{b}_{1,0}(i) = 0$ for $i = 1, 2, \dots, N$ (gradually one by one).
- Removing the interlayer connections of the outermost two layers with their subsequent layer, i.e., by simultaneously setting $\mathbf{b}_{-1,-2}(i) = \mathbf{b}_{2,1}(i) = 0$ for $i = 1, 2, \dots, N$ (gradually one by one).
- Removing the interlayer connections throughout the replica nodes across the five layers, i.e., by simultaneously setting $\mathbf{b}_{-1,-2}(i) = \mathbf{b}_{0,-1}(i) = \mathbf{b}_{1,0}(i) = \mathbf{b}_{2,1}(i) = 0$ for $i = 1, 2, \dots, N$ (gradually one by one).

Case (c) is the combination of the cases (a) and (b). The associated numerical results are delineated in figure 12. The left panel of figure 12 depicts the variation of E^{RIS} in the (ν, ϵ) parameter plane for three different types of demultiplexing schemes respectively in the upper, middle and lower panels. These three cases exhibit almost the similar qualitative behaviors. These three panels explicitly demonstrate that the critical value of ν (i.e., ν_c) required for the RIS of the pentaplex network reduces with increasing ϵ .

Finally, the right panel of figure 12 depicts the critical number of demultiplexed replica links ν_c which allow RIS in the (ϵ, η) parameter space for three different types of demultiplexing schemes respectively in figures 12(b), (d) and (f). The color bar represents the variation of ν_c . Similar to the left panel, here also the three figures exhibit almost the similar qualitative behaviors. Higher ν_c indicates more robustness of RIS with respect to the progressive demultiplexing. Notably, once again the intralayer coupling strength crucially influences ν_c . Clearly simultaneous increment of ϵ and η helps to enhance ν_c as shown in figure 12(f). Higher interlayer coupling strength η gives larger values of ν_c . This implies that increasing only the intralayer coupling strength in the five layers, one can make more persistent on the relay interlayer synchrony, even when a large number of replica connections are disconnected. So the monotonic dependence of ν_c on ϵ holds for all values of η .

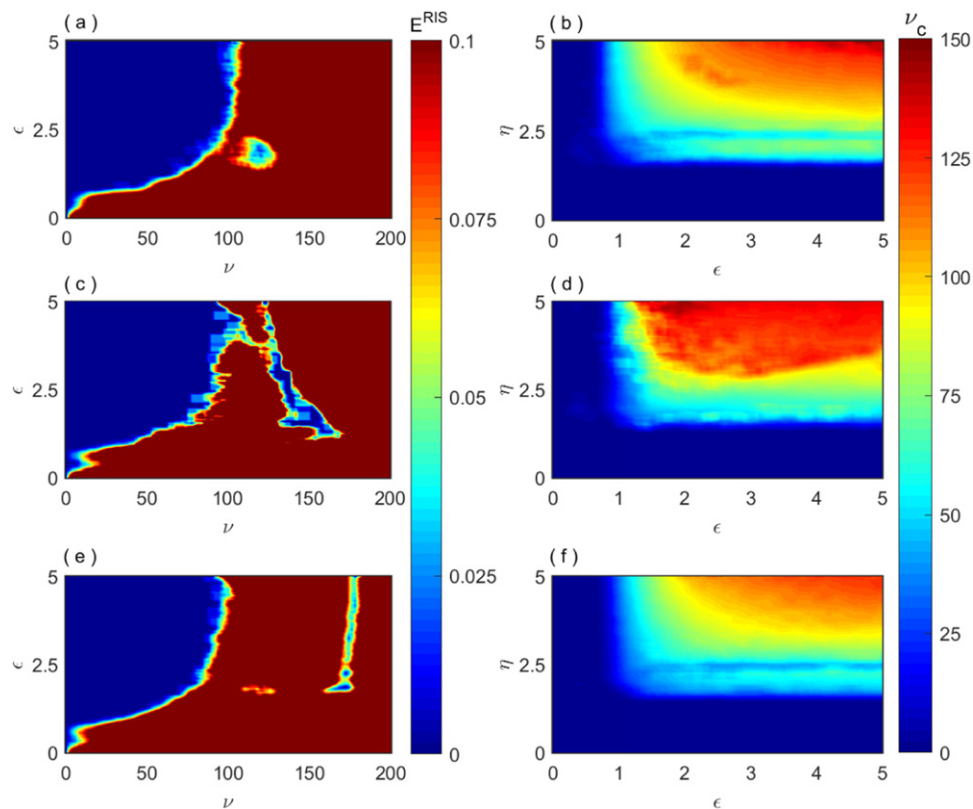


Figure 12. Left panel (a), (c) and (e): RIS region in the (ν, ϵ) parameter plane for $\eta = 3.5$, where the color bar represents the variation of E^{RIS} . Right panel (b), (d) and (f): Variation of the critical number of demultiplex node ν_c in the (ϵ, η) parameter plane. Upper (a) and (b), middle (c) and (d), and lower (e) and (f) panels are respectively plotted for three demultiplexing processes (a)–(c). Other parameter values: $\Delta\rho = 2.5$ and $p = 0.1$.

7. Conclusion and future perspectives

We have analytically studied RIS in a multiplex network consisting of $(2L + 1)$ layers induced by the dynamic relaying. With respect to the middlemost layer, the local dynamics of each node in the symmetric position layers are identical, while the middlemost layer has a parameter mismatch. We have derived the existence condition for this synchronisation state and found that the intralayer networks in the symmetric position layers should be identical for the emergence of interlayer synchronisation state. Next, we have generalised the local stability theory for a chain of layers and derived necessary-sufficient condition for the interlayer synchronisation state using master stability function approach. For global stability, we have used quadratic Lyapunov function and it gives a sufficient condition for RIS state. The robustness of the RIS state is theoretically investigated with respect to the progressive demultiplexing of replicas. For this, we have proposed a suitable demultiplexing process for RIS state in a chain of multiplex networks. We derived the variational equation transverse to the RIS manifold for demultiplexed systems.

To verify analytical results, we numerically simulate triplex and pentaplex networks consisting of chaotic dynamics (Rössler and Lorenz systems) in the nodes. Detailed transition scenarios from desynchrony to synchrony under the impact of interlayer and intralayer coupling strengths, variations of a system parameter in the relay layer are discussed in a wide range of different parameter spaces. Interestingly, we found that a common time-lag with an amplitude deviation is created between each replica of the symmetric positions layers and the mismatched relay layer due to the presence of parameter mismatched in the relay layer. This time-lag plays a role of dynamic relaying of the symmetric positions layers to establish an indirect coupling between them and thereby enhances the interlayer synchronisation between the symmetric positions layers. We do hope that similar analysis can be done for the even number layers, i.e., $2L$ number of layers. In this case, for invariance of the RIS state, the intralayer adjacency matrices of the symmetric positions layers with respect to a couple of layers in the middle should be identical and parameter mismatch should be introduced in the middlemost couple of layers [40].

Finally, we end our study with a brief discussion on what are the challenges in the context of this work that need to be addressed and are worth to studying in the future. First of all, we are not able to optimise the critical coupling strength for global stability, here our goal was to derive the sufficient condition for global stability of the RIS manifold \mathcal{S}^{RIS} . We have used quadratic polynomial approach for the construction of Lyapunov function which gives a critical value of the interlayer coupling strength far away from the local stability boundary. Therefore, it may be an interesting problem to derive the necessary and sufficient conditions for global asymptotic stability of synchronisation in multiplex networks. In such a case, an appropriate Lyapunov function need to be constructed which can optimise the coupling strength using the Lyapunov optimisation technique. Attention can also be paid to derive the necessary and sufficient conditions for the local stability of the RIS state.

The effect of dynamic relaying on the intralayer synchronisation state may be studied further. Precisely, in the case of RIS, a common time lag is created between the replica nodes of the symmetric position identical layers and the mismatched central layers leading to the interlayer lag synchronisation state. This interlayer lag synchronisation promotes RIS between indirect connected layers in the multiplex network. In other words, this time lag played a key role of dynamic relaying of the symmetric position layers to establish an indirect interaction among them, and resulting the enhancement of interlayer synchronisation in the symmetric position layers. In this present work, we did not provide any analytical justification for this interesting fact, also mathematical relation among this time lag, coupling strengths, and the amount of parameter mismatch is an interesting topic for future research.

Effect of time-delay in the interlayer connections on the emergence of RIS state is an another promising future research direction. In this study, time delay is emerged or created between the symmetric positions layers and the middlemost layer due to the parameter mismatch in the local dynamics of the nodes. Similar results may be observed between identical layers if time delay is introduced in the interlayer connections. In this context, the study on invariance and stability analysis of the RIS state under discrete-time individual node dynamics will be quite significant.

Acknowledgments

It is our pleasure to thank the editors and the anonymous referees for their careful reading, insightful suggestions and valuable remarks which improved the quality and readability of the paper. SNC is supported by the Council of Scientific & Industrial Research (CSIR) under

Project No. 09/093(0194)/2020-EMR-I JK is supported by the Russian Ministry of Science and Education Agreement No. 075-15-2020-808.

Appendix A. The proofs

A.1. Proof of lemma 1

Proof. If possible, let the interlayer synchronisation solution is an invariant solution in the multiplex network (3). For this purpose, consider at time $t = t_0$, where the state-variables of the i th node ($i = 1, 2, \dots, N$) of all the layers are equal, i.e., $\mathbf{x}_{l,i}(t_0) = \mathbf{x}_i(t_0)$ for $l = 0, \pm 1, \pm 2, \dots, \pm L$. To maintain the interlayer synchronisation state, the rate of change of each replica nodes should be identical at time t_0 , as their state variables are same at that time, otherwise, diverse rate of change in some replicas gives separate trajectories among themselves.

At this time instant, the rate of change of the i th node of all the layers are as follows,

$$\dot{\mathbf{x}}_{-L,i}(t_0) = f(\mathbf{x}_{-L,i}(t_0), \alpha_L) - \epsilon \sum_{j=1}^N \mathcal{L}_{ij}^{[-L]} G \mathbf{x}_{-L,j}(t_0), \quad (31a)$$

$$\dot{\mathbf{x}}_{l,i}(t_0) = f(\mathbf{x}_{l,i}(t_0), \alpha_{|l|}) - \epsilon \sum_{j=1}^N \mathcal{L}_{ij}^{[l]} G \mathbf{x}_{l,j}(t_0), \quad l = 0, \pm 1, \pm 2, \dots, \pm(L-1), \quad (31b)$$

$$\dot{\mathbf{x}}_{L,i}(t_0) = f(\mathbf{x}_{L,i}(t_0), \alpha_L) - \epsilon \sum_{j=1}^N \mathcal{L}_{ij}^{[L]} G \mathbf{x}_{L,j}(t_0). \quad (31c)$$

Thus to maintain the identical trajectory of each replica, we should have $\dot{\mathbf{x}}_{k,i}(t_0) = \dot{\mathbf{x}}_{l,i}(t_0)$, for $k \neq l$. But due to the parameter mismatch between the layers, we have,

$$f(\mathbf{x}_{l,i}(t_0), \alpha_{|k|}) \neq f(\mathbf{x}_{l,i}(t_0), \alpha_{|l|}). \quad (32)$$

Thus, the interlayer synchronisation state is not an invariant solution for the dynamical multiplex network (3). \square

A.2. Proof of lemma 3

Proof. To prove this invariance condition, consider the replica-wise initial conditions of the symmetric positions layers are identical, i.e., $\mathbf{x}_{l,i}(t_0) = \mathbf{x}_{-l,i}(t_0)$ for all $l = 1, 2, \dots, L$ and $i = 1, 2, \dots, N$. Now, we have to prove the condition for which $\dot{\mathbf{x}}_{l,i}(t_0) = \dot{\mathbf{x}}_{-l,i}(t_0)$ for all l . For that, we must have,

$$\sum_{j=1}^N \left[\mathcal{L}_{ij}^{[l]} - \mathcal{L}_{ij}^{[-l]} \right] G \mathbf{x}_{l,j}(t_0) = 0, \quad l = 1, 2, \dots, L \quad \text{and} \quad i = 1, 2, \dots, N. \quad (33)$$

In vectorial form, the above equation can be written as

$$\left[\mathcal{L}^{[l]} - \mathcal{L}^{[-l]} \right] \otimes G \mathbf{x}_l(t_0) = 0, \quad l = 1, 2, \dots, L. \quad (34)$$

Since, $\mathbf{x}_{l,i}(t_0)$ is an arbitrary initial condition of the i th node in the layer- l , and G is any arbitrary intralayer inner-coupling matrix, therefore, to satisfy equation (34), we need $\mathcal{L}^{[l]} = \mathcal{L}^{[-l]}$ for all $l = 1, 2, \dots, L$.

Therefore, we observe that if the replica-wise state variables of the symmetric positions layers are same, then they will remain same in the next time step, when the corresponding intralayer network architectures are identical. Proceeding with this argument for our interested time interval, we can argue that if the replica-wise initial conditions are same then the replica-wise state variables will remain same for all course of time. This shows that the RIS manifold is an invariant manifold of equation (3) if the intralayer adjacency matrices of the symmetric positions layers are identical. So due to the diffusive nature of the interlayer coupling function, if all replicas of the symmetric positions layers start with the same initial condition, then the replica-wise velocity profile becomes identical. This ensures that the RIS state is an invariant state. \square

A.3. Proof of lemma 4

Proof. We prove our desire result in terms of the invariance solution. If possible, let us assume that for a particular value of the interlayer coupling strength η , all the symmetric positions layers are in interlayer synchronisation state except one pair of layers, let $\pm k$ -layer. Therefore, $\mathbf{x}_{l,i}(t) = \mathbf{x}_{-l,i}(t)$ for all $l = 1, 2, \dots, k-1, k+1, \dots, L-1, L$. Also, there exists at least one replica nodes (let, i_1 th replica) in the $\pm k$ -layer such that $\mathbf{x}_{k,i_1}(t) \neq \mathbf{x}_{-k,i_1}(t)$ and $\dot{\mathbf{x}}_{k,i_1}(t) \neq \dot{\mathbf{x}}_{-k,i_1}(t)$.

Now the difference between the rate of change of the i_1 th replica nodes in the pair of layers $\pm k \mp 1$ can be written as,

$$\dot{\mathbf{x}}_{k-1,i_1}(t) - \dot{\mathbf{x}}_{-k+1,i_1}(t) = \eta H[\mathbf{x}_{k,i_1}(t) - \mathbf{x}_{-k,i_1}(t)]. \quad (35)$$

Since for the replica nodes i_1 in the pair of layers $\pm k$, we have $\mathbf{x}_{k,i_1}(t) \neq \mathbf{x}_{-k,i_1}(t)$ and $\eta \neq 0$, therefore, we have $\dot{\mathbf{x}}_{k-1,i_1}(t) \neq \dot{\mathbf{x}}_{-k+1,i_1}(t)$. Although, the initial conditions of the i_1 th replica nodes in the layers $\pm k \mp 1$ are identical, however, their non-identical rate of change gives the separate solution trajectories. In other words, the replica-wise desynchronisation motion in the $\pm k$ -layers propagates in the pair of layers $\pm k \mp 1$.

Similarly, the difference between the rate of change of the i_1 th replica nodes in the pair of layers $\pm k \pm 1$ can be written as,

$$\dot{\mathbf{x}}_{k+1,i_1}(t) - \dot{\mathbf{x}}_{-k-1,i_1}(t) = \eta H[\mathbf{x}_{k,i_1}(t) - \mathbf{x}_{-k,i_1}(t)]. \quad (36)$$

Therefore, in a similar reason the replica-wise desynchronisation motion of the nodes in layers $\pm k$ destroy the replica-wise synchronisation motion in the pair of layers $\pm k \pm 1$.

Likewise, the replica-wise desynchronisation motion in the layers $\pm k$, $\pm k \mp 1$, and $\pm k \pm 1$ will propagate to the layers $\pm k \mp 2$ and $\pm k \pm 2$ in the next time instance. Successively, within a short time-interval, the interlayer synchronisation motion of the distant layers will destroy due to the presence of one pair of layers which is not in the interlayer synchronisation state. Thus, we conclude that, the interlayer desynchronise motion never coexists with the interlayer synchronisation motion for the multiplex network (3). A replica-wise desynchronisation motion of one pair of layers is sufficient to destroy the other replica-wise synchronise motion.

Therefore, the interlayer synchronisations in the symmetric positions layers occur simultaneously. \square

A.4. Proof of lemma 14

Proof. First assume that the replica-wise initial conditions of the symmetric positions layers are identical, i.e., for the initial time instance $t = t_0$, $\mathbf{x}_{l,i}(t_0) = \mathbf{x}_{-l,i}(t_0)$ for all $i = 1, 2, \dots, N$

and $l = 1, 2, \dots, L$. Then for the replicas $i = i_1, i_2, \dots, i_m$ of the $\pm k$ th layers, the rate of change of the state variable at this time instance are respectively,

$$\begin{aligned}\dot{\mathbf{x}}_{k,i}(t_0) &= f(\mathbf{x}_{k,i}(t_0), \alpha_k) - \epsilon \sum_{j=1}^N \mathcal{L}_{ij}^{[k]} \mathbf{x}_{k,j}(t_0) + \eta H[\mathbf{x}_{k-1,i}(t_0) - \mathbf{x}_{k,i}(t_0)], \\ \dot{\mathbf{x}}_{-k,i}(t_0) &= f(\mathbf{x}_{-k,i}(t_0), \alpha_k) - \epsilon \sum_{j=1}^N \mathcal{L}_{ij}^{[k]} \mathbf{x}_{-k,j}(t_0) + \eta H[\mathbf{x}_{-k+1,i}(t_0) - \mathbf{x}_{-k,i}(t_0)].\end{aligned}\quad (37)$$

For the pair of $\pm(k+1)$ layers, we have the replica wise rate of change as

$$\begin{aligned}\dot{\mathbf{x}}_{k+1,i}(t_0) &= f(\mathbf{x}_{k+1,i}(t_0), \alpha_{k+1}) - \epsilon \sum_{j=1}^N \mathcal{L}_{ij}^{[k+1]} \mathbf{x}_{k+1,j}(t_0) + \eta H[\mathbf{x}_{k+2,i}(t_0) - \mathbf{x}_{k+1,i}(t_0)], \\ \dot{\mathbf{x}}_{-k-1,i}(t_0) &= f(\mathbf{x}_{-k-1,i}(t_0), \alpha_{k+1}) - \epsilon \sum_{j=1}^N \mathcal{L}_{ij}^{[k+1]} \mathbf{x}_{-k-1,j}(t_0) + \eta H[\mathbf{x}_{-k-2,i}(t_0) - \mathbf{x}_{-k-1,i}(t_0)],\end{aligned}\quad (38)$$

where $i \in \{i_1, i_2, \dots, i_m\}$. Similarly, for the pair of $\pm(k-1)$ layers, the replica wise rate of change can be written as

$$\begin{aligned}\dot{\mathbf{x}}_{k-1,i}(t_0) &= f(\mathbf{x}_{k-1,i}(t_0), \alpha_{k-1}) - \epsilon \sum_{j=1}^N \mathcal{L}_{ij}^{[k-1]} \mathbf{x}_{k-1,j}(t_0) + \eta H[\mathbf{x}_{k-1,i}(t_0) - \mathbf{x}_{k-1,i}(t_0)], \\ \dot{\mathbf{x}}_{-k+1,i}(t_0) &= f(\mathbf{x}_{-k+1,i}(t_0), \alpha_{k-1}) - \epsilon \sum_{j=1}^N \mathcal{L}_{ij}^{[k-1]} \mathbf{x}_{-k+1,j}(t_0) + \eta H[\mathbf{x}_{-k+2,i}(t_0) - \mathbf{x}_{-k+1,i}(t_0)],\end{aligned}\quad (39)$$

where $i \in \{i_1, i_2, \dots, i_m\}$. However, for $i \notin \{i_1, i_2, \dots, i_m\}$ of the pair of layers $l = \pm k, \pm k \pm 1, \pm k \mp 1$ or for all $i \in \{1, 2, \dots, N\}$ and $l \neq \pm k, \pm k \pm 1, \pm k \mp 1$, we have the rate of change of the replica connections as

$$\begin{aligned}\dot{\mathbf{x}}_{l,i}(t_0) &= f(\mathbf{x}_{l,i}(t_0), \alpha_l) - \epsilon \sum_{j=1}^N \mathcal{L}_{ij}^{[l]} \mathbf{x}_{l,j}(t_0) + \eta H[\mathbf{x}_{l+1,i}(t_0) + \mathbf{x}_{l-1,i}(t_0) - 2\mathbf{x}_{l,i}(t_0)], \\ \dot{\mathbf{x}}_{-l,i}(t_0) &= f(\mathbf{x}_{-l,i}(t_0), \alpha_l) - \epsilon \sum_{j=1}^N \mathcal{L}_{ij}^{[l]} \mathbf{x}_{-l,j}(t_0) + \eta H[\mathbf{x}_{-l+1,i}(t_0) + \mathbf{x}_{-l-1,i}(t_0) - 2\mathbf{x}_{-l,i}(t_0)].\end{aligned}\quad (40)$$

Therefore, for all the replica nodes of the symmetric positions layers, we have the identical rate of change, whenever their initial conditions are replica-wise identical. Hence, the RIS solution will be an invariant solution for such systematic progressive demultiplexing. \square

A.5. Proof of theorem 15

Proof. We perturb the i th node of the layer- l from its counterpart node in the layer- $(-l)$ with amount $\delta \mathbf{x}_{l,i}(t)$. Then the state variable of layer- l can be written as $\mathbf{x}_{l,i}(t) = \mathbf{x}_{-l,i}(t) + \delta \mathbf{x}_{l,i}(t)$.

Considering small perturbation $\delta \mathbf{x}_{l,i}(t)$ and expanding around equation (21) up to first order, the time-derivative of $\delta \mathbf{x}_{l,i}(t)$ can be written as

$$\begin{aligned} \delta \dot{\mathbf{x}}_{1,i}(t) &= \dot{\mathbf{x}}_{1,i}(t) - \dot{\mathbf{x}}_{-1,i}(t) = Jf(\mathbf{x}_{1,i}, \alpha_1) \delta \mathbf{x}_{1,i} - \epsilon \sum_{j=1}^N \mathcal{L}_{ij}^{[1]} G \delta \mathbf{x}_{1,j} \\ &\quad + \eta [-\mathbf{b}_{1,0}(i) H \delta \mathbf{x}_{1,i} + \mathbf{b}_{2,1}(i) H (\delta \mathbf{x}_{2,i} - \delta \mathbf{x}_{1,i})], \\ \delta \dot{\mathbf{x}}_{l,i}(t) &= \dot{\mathbf{x}}_{l,i}(t) - \dot{\mathbf{x}}_{-l,i}(t) = Jf(\mathbf{x}_{l,i}, \alpha_l) \delta \mathbf{x}_{l,i} - \epsilon \sum_{j=1}^N \mathcal{L}_{ij}^{[l]} G \delta \mathbf{x}_{l,j} \\ &\quad + \eta [\mathbf{b}_{l,l-1}(i) H (\delta \mathbf{x}_{l-1,i} - \delta \mathbf{x}_{l,i}) \\ &\quad + \mathbf{b}_{l+1,l}(i) H (\delta \mathbf{x}_{l+1,i} - \delta \mathbf{x}_{l,i})], \quad l = 2, 3, \dots, L-1, \\ \delta \dot{\mathbf{x}}_{L,i}(t) &= \dot{\mathbf{x}}_{L,i}(t) - \dot{\mathbf{x}}_{-L,i}(t) = Jf(\mathbf{x}_{L,i}, \alpha_L) \delta \mathbf{x}_{L,i} - \epsilon \sum_{j=1}^N \mathcal{L}_{ij}^{[L]} G \delta \mathbf{x}_{L,j} \\ &\quad + \eta \mathbf{b}_{L,L-1}(i) H (\delta \mathbf{x}_{L-1,i} - \delta \mathbf{x}_{L,i}), \end{aligned} \quad (41)$$

for $i = 1, 2, \dots, N$. In vectorial form, the above variational equation can be written in the form of equation (23).

ORCID iDs

Sarbendu Rakshit  <https://orcid.org/0000-0001-8479-5696>
 Fatemeh Parastesh  <https://orcid.org/0000-0002-0237-313X>
 Sayantan Nag Chowdhury  <https://orcid.org/0000-0002-0326-826X>
 Sajad Jafari  <https://orcid.org/0000-0002-6845-7539>
 Jürgen Kurths  <https://orcid.org/0000-0002-5926-4276>
 Dibakar Ghosh  <https://orcid.org/0000-0003-4832-5210>

References

- [1] Boccaletti S, Latora V, Moreno Y, Chavez M and Hwang D 2006 Complex networks: structure and dynamics *Phys. Rep.* **424** 175–308
- [2] Wang X F and Chen G 2003 Complex networks: small-world, scale-free and beyond *IEEE Circuits Syst. Mag.* **3** 6–20
- [3] Kivela M, Arenas A, Barthelemy M, Gleeson J P, Moreno Y and Porter M A 2014 Multilayer networks *J. Complex Netw.* **2** 203–71
- [4] Boccaletti S, Bianconi G, Criado R, del Genio C I, Gómez-Gardeñes J, Romance M, Sendiña-Nadal I, Wang Z and Zanin M 2014 The structure and dynamics of multilayer networks *Phys. Rep.* **544** 1–122
- [5] Newman M E J 2003 The structure and function of complex networks *SIAM Rev.* **45** 167–256
- [6] Strogatz S H 2000 From Kuramoto to Crawford: exploring the onset of synchronisation in populations of coupled oscillators *Physica D* **143** 1–20
- [7] Barrat A, Barthelemy M and Vespignani A 2008 *Dynamical Processes on Complex Networks* (Cambridge: Cambridge University Press)
- [8] Omel'chenko O E 2019 Travelling chimera states in systems of phase oscillators with asymmetric nonlocal coupling *Nonlinearity* **33** 611–42

- [9] Pikovsky A, Rosenblum M and Kurths J 2003 *Synchronisation: A Universal Concept in Nonlinear Sciences* (Cambridge: Cambridge University Press)
- [10] Omelchenko I, Omel'chenko O E, Hövel P and Schöll E 2013 When nonlocal coupling between oscillators becomes stronger: patched synchrony or multichimera states *Phys. Rev. Lett.* **110** 224101
- [11] Ghosh D, Frasca M, Rizzo A, Majhi S, Rakshit S, Alfaro B K and Boccaletti S 2021 Synchronisation in time-varying networks (arXiv:2109.07618)
- [12] Arenas A, Díaz-Guilera A, Kurths J, Moreno Y and Zhou C 2008 Synchronisation in complex networks *Phys. Rep.* **469** 93–153
- [13] Boccaletti S, Kurths J, Osipov G, Valladares D L and Zhou C S 2002 The synchronisation of chaotic systems *Phys. Rep.* **366** 1–101
- [14] Pecora L M and Carroll T L 1990 Synchronisation in chaotic systems *Phys. Rev. Lett.* **64** 821
- [15] Chowdhury S N, Majhi S, Ozer M, Ghosh D and Perc M 2019 Synchronisation to extreme events in moving agents *New J. Phys.* **21** 073048
- [16] Nikitin D, Omelchenko I, Zakharova A, Avetyan M, Fradkov A L and Schöll E 2019 Complex partial synchronisation patterns in networks of delay-coupled neurons *Phil. Trans. R. Soc. A* **377** 20180128
- [17] Jalan S and Singh A 2016 Cluster synchronisation in multiplex networks *Europhys. Lett.* **113** 30002
- [18] Nag Chowdhury S, Rakshit S, Buldú J M, Ghosh D and Hens C 2021 Antiphase synchronisation in multiplex networks with attractive and repulsive interactions *Phys. Rev. E* **103** 032310
- [19] Zhang X, Boccaletti S, Guan S and Liu Z 2015 Explosive synchronisation in adaptive and multilayer networks *Phys. Rev. Lett.* **114** 038701
- [20] Majhi S, Perc M and Ghosh D 2016 Chimera states in uncoupled neurons induced by a multilayer structure *Sci. Rep.* **6** 39033
- [21] Majhi S, Perc M and Ghosh D 2017 Chimera states in a multilayer network of coupled and uncoupled neurons *Chaos* **27** 073109
- [22] Maksimenko V A, Makarov V V, Bera B K, Ghosh D, Dana S K, Goremyko M V, Frolov N S, Koronovskii A A and Hramov A E 2016 Excitation and suppression of chimera states by multiplexing *Phys. Rev. E* **94** 052205
- [23] Gambuzza L V, Frasca M and Gómez-Gardeñes J 2015 Intra-layer synchronisation in multiplex networks *Europhys. Lett.* **110** 20010
- [24] Sevilla-Escoboza R, Sendiña-Nadal I, Leyva I, Gutiérrez R, Buldú J M and Boccaletti S 2016 *Chaos* **26** 065304
- [25] Drauschke F, Sawicki J, Berner R, Omelchenko I and Schöll E 2020 Effect of topology upon relay synchronisation in triplex neuronal networks *Chaos* **30** 051104
- [26] Rakshit S, Majhi S, Bera B K, Sinha S and Ghosh D 2017 Time-varying multiplex network: intralayer and interlayer synchronisation *Phys. Rev. E* **96** 062308
- [27] Rakshit S, Bera B K, Bollt E M and Ghosh D 2020 Intralayer synchronisation in evolving multiplex hypernetworks: analytical approach *SIAM J. Appl. Dyn. Syst.* **19** 918–63
- [28] Majhi S, Kapitaniak T and Ghosh D 2019 Solitary states in multiplex networks owing to competing interactions *Chaos* **29** 013108
- [29] Kheowan O U, Mihaliuk E, Blasius B, Sendiña-Nadal I and Showalter K 2007 Wave mediated synchronisation of nonuniform oscillatory media *Phys. Rev. Lett.* **98** 074101
- [30] Osipov G V, Pikovsky A S, Rosenblum M G and Kurths J 1997 Phase synchronisation effects in a lattice of nonidentical Rössler oscillators *Phys. Rev. E* **55** 2353
- [31] So P, Cotton B C and Barreto E 2008 Synchronisation in interacting populations of heterogeneous oscillators with time-varying coupling *Chaos* **18** 037114
- [32] Plotnikov S A, Lehnert J, Fradkov A L and Schöll E 2016 Synchronisation in heterogeneous FitzHugh–Nagumo networks with hierarchical architecture *Phys. Rev. E* **94** 012203
- [33] Barreto E, Hunt B, Ott E and So P 2008 Synchronisation in networks of networks: the onset of coherent collective behavior in systems of interacting populations of heterogeneous oscillators *Phys. Rev. E* **77** 036107
- [34] Berner R, Sawicki J and Schöll E 2020 Birth and stabilisation of phase clusters by multiplexing of adaptive networks *Phys. Rev. Lett.* **124** 088301
- [35] Ruzzene G, Omelchenko I, Sawicki J, Zakharova A, Schöll E and Andrzejak R G 2020 Remote pacemaker control of chimera states in multilayer networks of neurons *Phys. Rev. E* **102** 052216

- [36] Blaha K A, Huang K, Della R F, Pecora L, Hossein Z M and Sorrentino F 2019 Cluster synchronisation in multilayer networks: a fully analog experiment with LC oscillators with physically dissimilar coupling *Phys. Rev. Lett.* **122** 014101
- [37] Della Rossa F, Pecora L, Blaha K, Shirin A, Klickstein I and Sorrentino F 2020 Symmetries and cluster synchronisation in multilayer networks *Nat. Commun.* **11** 3179
- [38] Sorrentino F, Pecora L and Trajković L L 2020 Group consensus in multilayer networks *IEEE Trans. Netw. Sci. Eng.* **7** 2016–26
- [39] Leyva I, Sevilla-Escoboza R, Sendiña-Nadal I, Gutiérrez R, Buldú J M and Boccaletti S 2017 Inter-layer synchronisation in non-identical multi-layer networks *Sci. Rep.* **7** 45475
- [40] Banerjee R, Ghosh D, Padmanaban E, Ramaswamy R, Pecora L M and Dana S K 2012 Enhancing synchrony in chaotic oscillators by dynamic relaying *Phys. Rev. E* **85** 027201
- [41] Menara T, Qin Y, Bassett D S and Pasqualetti F 2021 Relay interactions enable remote synchronisation in networks of phase oscillators *IEEE Control Syst. Lett.* **6** 500–5
- [42] Leyva I, Sendiña-Nadal I, Sevilla-Escoboza R, Vera-Avila V P, Chholak P and Boccaletti S 2018 Relay synchronisation in multiplex networks *Sci. Rep.* **8** 8629
- [43] Sawicki J, Omelchenko I, Zakharova A and Schöll E 2018 Delay controls chimera relay synchronisation in multiplex networks *Phys. Rev. E* **98** 062224
- [44] Rybalova E, Strelkova G, Schöll E and Anishchenko V 2020 Relay and complete synchronisation in heterogeneous multiplex networks of chaotic maps *Chaos* **30** 061104
- [45] Winkler M, Sawicki J, Omelchenko I, Zakharova A, Anishchenko V and Schöll E 2019 Relay synchronisation in multiplex networks of discrete maps *Europhys. Lett.* **126** 50004
- [46] Rakshit S, Bera B K and Ghosh D 2020 Invariance and stability conditions of interlayer synchronisation manifold *Phys. Rev. E* **101** 012208
- [47] Golub G H and Van Loan C F 1996 *Matrix Computations* (Baltimore, MD: Johns Hopkins University Press)
- [48] Pecora L M and Carroll T L 1998 Master stability functions for synchronised coupled systems *Phys. Rev. Lett.* **80** 2109
- [49] Polyak B and Shcherbakov P 2017 Lyapunov functions: an optimisation theory perspective *IFAC-PapersOnLine* **50** 7456–61
- [50] Neely M J 2010 Stochastic network optimisation with application to communication and queueing systems *Synthesis Lectures on Communication Networks* vol 3 (San Rafael, CA: Morgan & Claypool) pp 1–211
- [51] Sanz Serna J M and Zygalakis K C 2021 The connections between Lyapunov functions for some optimisation algorithms and differential equations *SIAM J. Numer. Anal.* **59** 1542–65
- [52] Hauswirth A, Bolognani S, Hug G and Dörfler F 2020 Timescale separation in autonomous optimisation *IEEE Trans. Automat. Contr.* **66** 611–24
- [53] The codes for numerical simulations are available at <https://github.com/Sarbendu-Rakshit/Relay-interlayer-synchronisation>
- [54] Rosenblum M G, Pikovsky A S and Kurths J 1997 From phase to lag synchronisation in coupled chaotic oscillators *Phys. Rev. Lett.* **78** 4193
- [55] Huang L, Chen Q, Lai Y C and Pecora L M 2009 Generic behavior of master-stability functions in coupled nonlinear dynamical systems *Phys. Rev. E* **80** 036204